Breastmilk-promoted bifidobacteria produce aromatic lactic acids in the infant gut

Martin F. Laursen[1#], Mikiyasu Sakanaka[1,2], Nicole von Burg[3], Daniel Andersen[4], Urs Mörbe[3], Aymeric Rivollier[3], Ceyda T. Pekmez[5], Janne Marie Moll[4], Kim F. Michaelsen[5], Christian Mølgaard[5], Mads Vendelbo Lind[5], Lars O. Dragsted[5], Takane Katayama[2,6], Henrik L. Frandsen[1], Anne Marie Vinggaard[1], Martin I. Bahl[1], Susanne Brix[4], William Agace[3], Tine R. Licht[1*] and Henrik M. Roager[1,5#*]

[#] These authors contributed equally

Affiliations

[1] National Food Institute, Technical University of Denmark, Kgs. Lyngby, Denmark

[2] Faculty of Bioresources and Environmental Sciences, Ishikawa Prefectural University, Ishikawa 921-8836, Japan

[3] Department of Health Technology, Technical University of Denmark, Kgs. Lyngby, Denmark

[4] Department of Biotechnology and Biomedicine, Technical University of Denmark, Kgs. Lyngby, Denmark

[5] Department of Nutrition, Exercise and Sports, University of Copenhagen, Frederiksberg C, Denmark

[6] Graduate school of Biostudies, Kyoto University, Kyoto 606-8502, Japan

Correspondence

* Tine R. Licht, Tel. + 45 35887186, trli@food.dtu.dk, Kemitorvet, 2800 Kongens Lyngby, Denmark

* Henrik M. Roager, Tel. + 45 35324928, hero@nexs.ku.dk, Rolighedsvej 30, 1958 Frederiksberg C, Denmark

ABSTRACT

Breastfeeding profoundly shapes the infant gut microbiota, which is critical for early life immune development. However, few breastmilk-dependent microbial metabolites mediating host-microbiota interactions are currently known. We here demonstrate that breastmilk-promoted *Bifidobacterium* species convert aromatic amino acids (tryptophan, phenylalanine and tyrosine) into their respective aromatic lactic acids (indolelactate, phenyllactate and 4-hydroxyphenyllactate) via a previously unrecognised aromatic lactate dehydrogenase. By longitudinal profiling of the gut microbiota composition and metabolome of stool samples of infants obtained from birth until 6 months of age, we show that stool concentrations of aromatic lactic acids is determined by the abundance of human milk oligosaccharide degrading *Bifidobacterium* species containing the aromatic lactate dehydrogenase. Finally, we demonstrate that stool concentrations of *Bifidobacterium*-derived indolelactate are associated with the capacity of infant stool samples to activate the aryl hydrocarbon receptor, a receptor important for maintenance of intestinal homeostasis and immune system development. These findings open up new directions towards understanding the role of breastmilk-promoted *Bifidobacterium* in mediating host-microbiota interactions in early life.

INTRODUCTION

Human breastmilk is a perfectly adapted nutritional supply for the infant[1]. Breastfeeding provides children with important short-term protection against infections, and may also provide long-term metabolic benefits[1,2]. These benefits may partly be mediated through the gut microbiota, since breastfeeding is the strongest determinant of gut microbiota composition and function during infancy[3–5]. Human breastmilk contains human milk oligosaccharides (HMOs), which are complex, highly abundant sugars serving as substrates for specific microbes including certain species of *Bifidobacterium*[6]. This co-evolution between bifidobacteria and the host, mediated by HMOs, to a large extent directs the colonization of the gut in early life, which has critical impact on the immune system[7]. Depletion of specific microbes, including *Bifidobacterium,* in early life has been associated with increased risk of allergy and asthma development in childhood[8,9], and is suggested to compromise immune function and lead to increased susceptibility to infectious disease[10,11]. Despite *Bifidobacterium* dominating the gut of breastfed infants and being widely acknowledged as beneficial, mechanistic insights on the contribution of these bacteria and their metabolites to immune development during infancy remain limited. Recent studies show that microbial aromatic amino acid metabolites including tryptophan-derived indoles[12], via activation of the aryl hydrocarbon receptor (AhR), can fortify the intestinal barrier[13,14], protect against pathogenic infections[15,16] and influence host metabolism[13,17,18], which makes this group of microbial metabolites of particular interest in the context of early life.

Here, we show that breastmilk-promoted *Bifidobacterium* species, via a previously unrecognised aromatic lactate dehydrogenase, produce aromatic lactic acids including indolelactate (ILA) in substantial amounts in the infant gut, and that stool concentrations of this metabolite are associated with the capacity of infant stool to activate AhR, which is known to impact immune development in early life.

RESULTS

Bifidobacterium species associate with aromatic amino acid catabolites during late infancy

To explore interactions between breastfeeding status, gut microbial composition and metabolism of aromatic amino acid in early life, we employed 16S rRNA amplicon sequencing to infer gut microbiota composition and a targeted ultra-performance liquid chromatography mass spectrometry (UPLC-MS) metabolomics approach to quantify 19 aromatic amino acids and derivatives thereof (**Supplementary Table 1**) in stool samples from 59 healthy Danish infants from the SKOT I cohort[19]. The SKOT I infants included were born full term, 9.1 ± 0.3 (mean ± SD) months of age at sampling, and 40.7% were still partially breastfed (**Supplementary Data 1a,b**). After stratification of the 9 months old infants based on breastfeeding status (partially breastfed versus weaned), Principal Coordinates Analysis (PCoA) of weighted UniFrac distances showed a significant separation across the first PC-axis ($r^2 = 0.093$, $p < 0.001$, Adonis test; **Fig. 1a**), which was due to an increasing gradient in relative abundance of *Bifidobacterium* in breastfed infants ($r^2 = 0.397$, $p < 0.001$, Adonis test; **Fig. 1b**). Other metadata (age, gender, mode of delivery, current formula intake and age of introduction to solid foods) did not explain gut microbiota variation to the same degree as breastfeeding status (**Supplementary Data 1c,d**). Principal Component Analysis (PCA) of faecal aromatic amino acid metabolite concentrations also revealed separation according to breastfeeding status, which was largely driven by three aromatic lactic acids, 4-hydroxyphenyllactic acid (4-OH-PLA), phenyllactic acid (PLA) and indolelactic acid (ILA) (**Fig. 1c**). Correlation analysis revealed that *Bifidobacterium*, but no other bacterial genera, were significantly associated with faecal concentrations of all three aromatic lactic acids (4-OH-PLA, PLA and ILA), in addition to indolealdehyde (IAld) (**Fig. 1d** and **Supplementary Data 1e**). *Bifidobacterium* species (**Supplementary Fig. 1a** and **Supplementary Data 1f**) significantly enriched in the breastfed infants; *B. longum*, *B. bifidum*, and *B. breve*, were positively associated with the faecal concentrations of aromatic lactic acids (4-OH-PLA, PLA and ILA) and IAld (cluster 1 in **Fig. 1e**), but negatively associated with the faecal concentrations of aromatic propionic acids, aromatic amino acids and to a lesser degree with aromatic acetic acids (cluster 2 in **Fig. 1e**). In contrast, post weaning type *Bifidobacterium* species, including *B. adolescentis*, *B. animalis/pseudolongum* and *B. catenulatum* group[20,21], were not significantly associated with aromatic lactic acids nor breastfeeding status (**Fig. 1e**). These associations were in agreement with the observation that the concentrations of the three aromatic lactic acids were higher in the faeces of breastfed than in weaned infants (**Supplementary Fig. 1b**). Furthermore, the abundances of the three aromatic lactic acids in infant urine (**Supplementary Fig. 2-4**) showed similar positive associations between relative abundances of breastmilk-promoted *Bifidobacterium* species (**Supplementary Fig. 1c**). In addition, faecal and urinary levels of ILA were positively correlated ($rho = 0.68$, $p < 0.0001$), showing that faecal levels of this metabolite are reflected systemically. Consistently, urine abundance of ILA, but not of PLA and 4-OH-PLA, were significantly higher in breastfed compared to weaned infants (**Supplementary Fig. 1b**). Together, this suggests that specific breastmilk-promoted *Bifidobacterium* species in the gut of infants convert aromatic amino acids to the corresponding aromatic lactic acids (**Fig. 1f**).

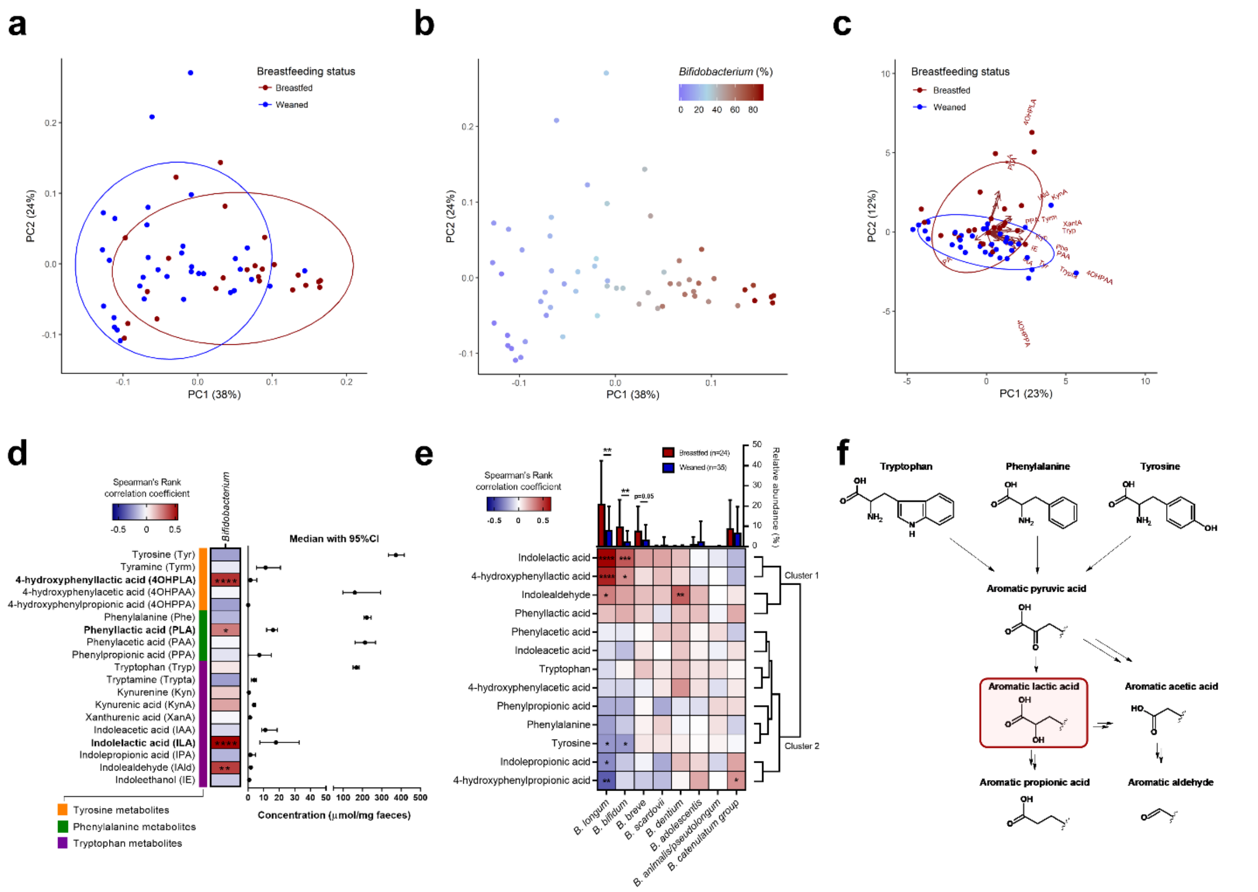

Figure 1. Breastfeeding associates with gut microbiota composition and aromatic amino acid catabolism in 9 months old infants

a-b, Principal coordinate analysis plots of weighted UniFrac distances based on OTUs from faecal samples of 9 months old infants participating in the SKOT cohort (n = 59). Samples are coloured according to (a) breastfeeding status with ellipses indicating 80%CI of data points for partially breastfed (red, n = 24) and weaned (blue, n = 35) infants or (b) relative abundance of the genus *Bifidobacterium.*

c, Principal component analysis plot of concentrations (µmol/mg faeces) of aromatic amino acids and their catabolites in SKOT faecal samples, coloured according to breastfeeding status with ellipses indicating 80%CI of data points for breastfed (red, n = 24) and weaned (blue, n = 35) infants. Loadings are shown with arrows. See abbreviations in (d).

d, Heatmap illustrating Spearman's Rank correlation coefficients between the relative abundance of *Bifidobacterium* and concentrations of aromatic amino acids and their catabolites in SKOT faecal samples (n=59). The concentration of each metabolite (µmol/mg faeces) is presented as the median with 95%CI.

e, Heatmap illustrating hierarchical clustering of Spearman's Rank correlation coefficients between the relative abundance of the different *Bifidobacterium* species and selected microbial-derived aromatic amino acid catabolites. Bar plots are showing relative abundance (mean+SD) of the *Bifidobacterium* spp., stratified according to breastfeeding status, with statistical significance evaluated by Mann-Whitney *U* test.

f, The pathway of aromatic amino acid catabolism by gut microbes (modified from Smith and Macfarlane 1996[95], Smith and Macfarlane 1997[96], and Zelante *et al*. 2013[16]). Asterisks indicate statistical significance: * p<0.05, ** p<0.01, *** p<0.001, **** p<0.0001.

See also **Supplementary Figure 1-4**.

Bifidobacterium species produce aromatic lactic acids *in vitro*

To confirm the ability of *Bifidobacterium* species detected in infants to produce aromatic lactic acids, *Bifidobacterium* type strains were grown anaerobically in a medium containing all three aromatic amino acids with either glucose or HMOs as sole carbohydrate sources. Analyses of culture supernatants revealed that ILA, PLA and 4-OH-PLA were produced mainly by *B. bifidum, B. breve*, *B. longum* subsp. *longum*, *B. longum* subsp*. infantis* and *B. scardovii* (**Fig. 2a**), in accordance with the associations observed in the 9 months old infants (**Fig. 1e**). Other *Bifidobacterium* species, namely *B. adolescentis*, *B. animalis* subsp*. lactis*, *B. animalis* subsp. *animalis, B. dentium, B. catenulatum, B. pseudocatenulatum, B. pseudolongum* subsp. *pseudolongum* produced only low amounts of these metabolites **(Fig. 2a**). The ability of *Bifidobacterium* species to produce high levels of the aromatic lactic acids was generally convergent with the ability to utilize HMOs as carbohydrate source (**Fig. 2a**), supporting the link between breastmilk-promoted bifidobacteria and production of aromatic lactic acids. None of the downstream products of the aromatic lactic acids (**Fig. 1f**) were detected in any of the culture supernatants.

An aromatic lactate dehydrogenase is responsible for the aromatic lactic acid production

Since it has been reported that an L-lactate dehydrogenase (LDH) in *Lactobacillus* spp. can convert phenylpyruvic acid to PLA[22], we hypothesized that a corresponding enzyme was present in *Bifidobacterium* species. Alignment and phylogenetic analysis of all genes annotated as *ldh* in the *Bifidobacterium* type strains included in this study, revealed four clusters (**Fig. 2b**). Whereas all *Bifidobacterium* genomes contain an *ldh* responsible for conversion of pyruvate to lactate (here designated as type 1 *ldh*) in the bifidobacterial fructose-6-phosphate shunt[23,24], some species have an extra *ldh*, here designated as type 2, type 3 and type 4, respectively. In agreement with the *in vitro* fermentations (**Fig. 2a**), all prominent aromatic lactic acid-producing *Bifidobacterium* species contain the type 4 *ldh*. Interestingly, genomic analysis of the *Bifidobacterium* type strains revealed that the type 4 *ldh* gene is part of a genetic element containing an amino acid transaminase gene (suspected to be responsible for converting the aromatic amino acids into aromatic pyruvic acids) and a haloacid dehydrogenase gene (of unknown importance) (**Supplementary Fig. 5**), which has been indicated to constitute an operon in *B. breve*[25]. Cloning of the type 4 *ldh* gene from *B. longum* subsp. *infantis*^{T} into a vector transformed into *E. coli* revealed that the expression of the type 4 *ldh* gene indeed resulted in the appearance of PLA, 4-OH-PLA and ILA in the culture supernatant (**Fig. 2c**). To verify the type 4 *ldh* dependent production of aromatic lactic acids in *Bifidobacterium* species, we generated a type 4 *ldh* insertional mutant strain by homologous recombination in *B. longum* subsp. *longum* 105-A (**Supplementary Fig. 6**), a genetically tractable strain containing the type 4 LDH (**Supplementary Fig. 7**)[26,27]. Cultivation of the wild-type (WT), the type 4 *ldh* mutant strain and a complemented type 4 *ldh* mutant strain in a medium containing the three aromatic amino acids (**Supplementary Fig. 6**) confirmed that type 4 *ldh* disruption did not impair growth (**Fig. 2d**). ILA, PLA and 4-OH-PLA accumulated in the supernatant of the WT and of the complemented type 4 *ldh* mutant strains, but not in the type 4 *ldh* mutant (**Fig. 2e**). Importantly, the type 4 *ldh* mutant was not significantly compromised in its ability to convert pyruvate to lactate (**Fig. 2e**), supporting the distinct role of type 4 *ldh* in converting aromatic pyruvic acids.

Purification and characterization of the recombinant type 4 LDH enzyme revealed that it had a mass of 33.9 kDa (**Supplementary Fig. 8a**), while the native molecular mass was estimated to be 72.9 kDa by size exclusion chromatography, indicating dimer formation in solution **(Supplementary Fig. 8b**). No metal requirement was observed, the optimal pH was 8.0-8.5 and the enzyme was most stable at 37°C (**Supplementary Fig. 8c-e**). Heterotrophic effects were neither observed for fructose-1,6-bisphosphate (an allosteric effector for type 1 LDH) nor for several intermediates for aromatic amino acid synthesis[23,24] (**Supplementary Fig. 9**). However, we found that phosphate served as a positive effector suggesting that type 4 LDH is an intracellular enzyme (**Supplementary Fig. 10a-c**). Assay at the different phosphate concentrations revealed the type 4 LDH is a *K*-type allosteric enzyme (**Supplementary Fig. 10b,c**). The catalytic rate (k_{cat}) was moderate to high for the aromatic pyruvic acid substrates, but very low for pyruvate (**Fig. 2f,g**), in accordance with the non-impaired lactate production observed for the type 4 *ldh* mutant (**Fig. 2e**). Production of ILA, PLA and 4-OH-PLA from the respective aromatic pyruvic acid substrates was verified by high-performance liquid chromatography (HPLC) (**Supplementary Fig. 10d**). The enzyme showed highest affinity (lowest $K_{0.5}$) for indole pyruvic acid, but highest catalytic rate for 4-OH-phenyl pyruvic acid in the presence of 100 mM phosphate (**Fig. 2f,g**). However, maximal catalytic efficiency ($k_{cat}/K_{0.5}$) was observed for indole pyruvic acid (190 s^{-1} mM^{-1}), followed by 4-OH-phenyl pyruvic acid (16 s^{-1} mM^{-1}) and phenyl pyruvic acid (11 s^{-1} mM^{-1}), suggesting preference for indole pyruvic acid. The observed Hill coefficient (n_H = 1-1.4) for all substrates indicate weak positive cooperativity under the conditions tested. Collectively, these results show that the type 4 *ldh* gene encodes an aromatic lactate dehydrogenase responsible for the production of ILA, PLA and 4-OH-PLA in *Bifidobacterium* species associated with breastfeeding. We therefore suggest that the type 4 *ldh* gene should be re-classified as an aromatic lactate dehydrogenase gene (*aldh*).

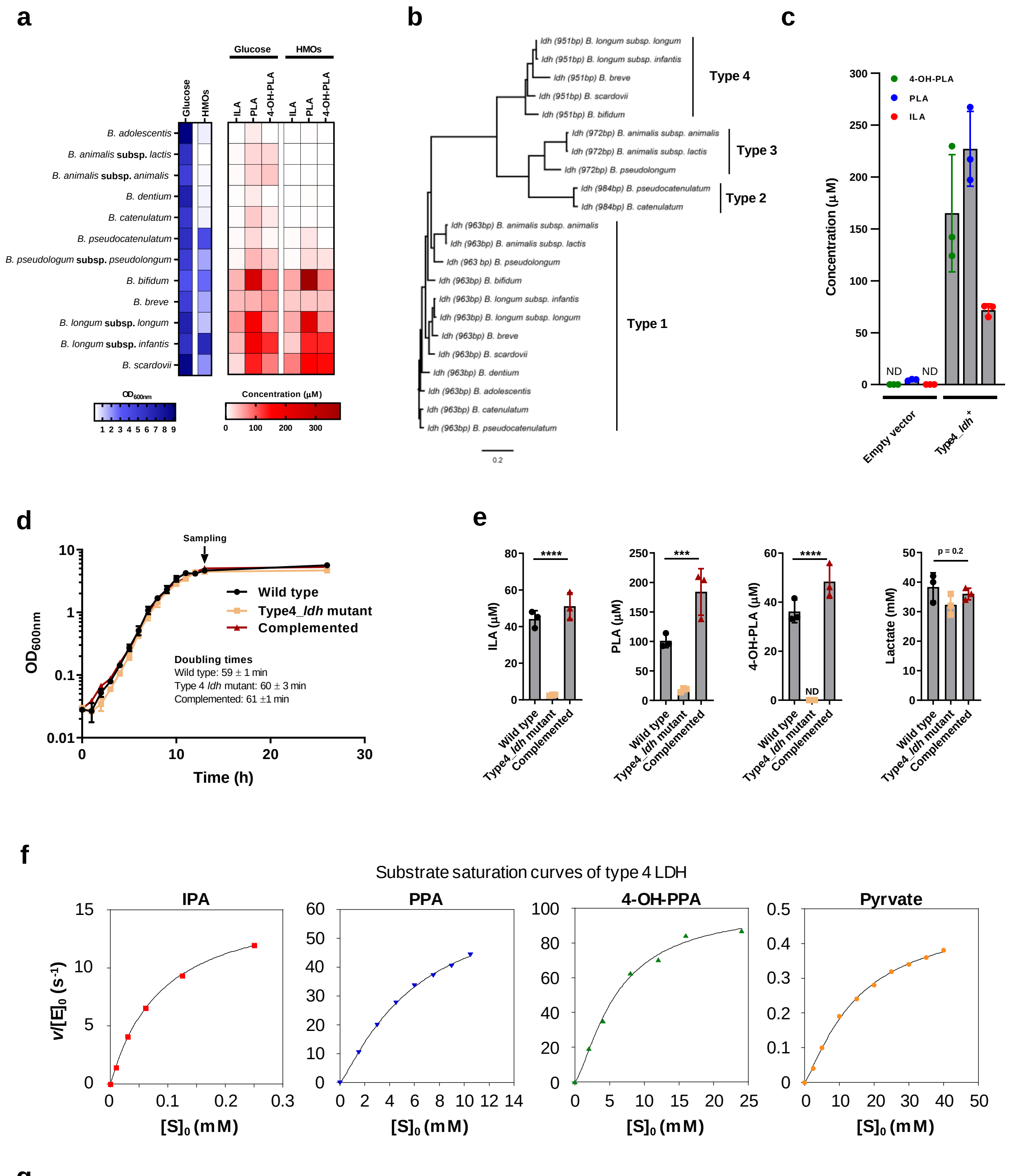

g

Kinetic parameters (Hill equation) of type 4 LDH

Substrate	$K_{0.5}$ (mM)	k_{cat} (s^{-1})	$k_{cat}/K_{0.5}$ (s^{-1} mM^{-1})	n_H (Hill coefficient)
IPA	0.08 ± 0.01	15.21 ± 1.01	193.73	1.05 ± 0.02
PPA	5.96 ± 0.06	64.22 ± 2.38	10.77	1.20 ± 0.01
4-OH-PPA	6.61 ± 0.93	103.89 ± 4.32	15.83	1.39 ± 0.01
Pyruvate	14.88 ± 0.48	0.47 ± 0.03	0.03	1.28 ± 0.05

Figure 2. *Bifidobacterium* species produce aromatic lactic acids via an aromatic lactate dehydrogenase
a, *In vitro* production of indolelactic acid (ILA), phenyllactic acid (PLA) and 4-hydroxyphenyllactic acid (4-OH-PLA)

by *Bifidobacterium* spp. type strains in modified MRS medium (MRSc) with 2% (w/v) glucose or a mix human milk oligosaccharides as sole carbohydrate source. For the type strains of *B. adolescentis*, *B. animalis* subsp. *animalis*, *B. animalis* subsp. *lactis*, *B. dentium* and *B. catenulatum* no or very poor growth (OD_{600nm} < 0.4) was observed with HMOs as carbohydrate source. Mean of three biological replicates is shown.
b, Neighbor-Joining phylogenetic tree of all genes in the *Bifidobacterium* spp. type strains annotated as L-lactate dehydrogenases (*ldh*). The four clusters are designated type 1-4.
c, Production of ILA, PLA and 4-OH-PLA by *E. coli* LMG194 cells transformed with an inducible vector lacking (empty vector) or containing the type 4 *ldh* (Type4_*ldh*$^+$) from *B. longum* subsp. *infantis* DSM 20088^T in LB-medium 5 h post-induction of gene expression by addition of L-arabinose and supplementation with the aromatic pyruvic acids (indolepyruvate, phenylpyruvate and 4-OH-phenylpyruvate). Bars show mean ± SD of three biological replicates.
d, Growth curves of *Bifidobacterium longum* subsp. *longum* 105-A (wild type), its isogenic insertional type 4 *ldh* mutant (Type4_*ldh* mutant) and the type 4 *ldh* mutant strain complemented with the type 4 *ldh* gene (Complemented). Curves show mean ± SD of three biological replicates and doubling times reported as mean ± SD.
e, Production of ILA, PLA, 4-OH-PLA and lactate by wild type, Type4_*ldh* mutant and the complemented strain in early stationary phase cultures. Bars show mean ± SD of three biological replicates. Statistical significance was evaluated by one-way ANOVA, with * p<0.05, ** p<0.01, *** p<0.001, **** p<0.0001.
f-g, Enzyme kinetics of the type 4 lactate dehydrogenase. **f**, substrate saturation curves of type 4 LDH with indole pyruvate, phenylpyruvate, 4-OH-phenylpyruvate or pyruvate as substrates. Data is one representative of two independent assays. **g**, kinetic parameters of type 4 LDH with the different substrates. Data are mean ± SD of two independent assays.
ND, not detected

See also **Supplementary Figure 5-10**.

Bifidobacterium species govern aromatic lactic acid profiles during early infancy

To study the dynamics of *Bifidobacterium* species establishment and aromatic lactic acids in infants, we established the Copenhagen Infant Gut (CIG) cohort including 25 healthy breast- or mixed fed infants, which were sampled every 2-4 weeks from birth until the age of 6 months (**Supplementary Data 2a**) for microbiome profiling and targeted metabolite quantification including aromatic lactic acids (**Supplementary Fig. 11** and **Supplementary Table 2**). A total of 145 operational taxonomic units (OTUs) were detected by 16S rRNA amplicon sequencing, however, collapsing of OTUs with identical taxonomic classifications and using a cut-off of average relative abundance of 0.1%, resulted in the identification of 39 bacterial species/taxa, representing 97.5% of the total community (**Supplementary Fig. 11a** and **Supplementary Data 2b**). As expected, the gut microbiota was highly dominated by *Bifidobacterium* (average of 64.2 %) and among the top 10 dominating taxa, *B. longum* (38.5 %), *B. breve* (9.1 %), *B. bifidum* (7.9 %), *B. catenulatum* group (6.4 %) and *B. dentium* (1.7 %) were found (**Supplementary Fig. 11a**), with the remaining *Bifidobacterium* spp. being assigned to *B. scardovii* (0.24 %), *B. adolescentis* (0.15 %) and *B. animalis/pseudolongum* (0.10 %) (**Supplementary Data 2b,c**). Although the relative abundance of *Bifidobacterium* increased with time, on average the microbial composition and Shannon diversity did not change dramatically during the six months (**Supplementary Fig. 11b**). However, the subject specific gut microbiota profiles revealed a highly individual species composition (**Supplementary Fig. 11c**) and 48% of the variation in community structure was explained by subject (weighted UniFrac, r^2 = 0.48, p < 0.001, Adonis, **Supplementary Fig. 12a,b**). Indeed, the difference in microbial community structure between faecal samples were primarily driven by the abundance of *Bifidobacterium* as assessed by PCoA of weighted UniFrac distances (r^2

= 0.48, p < 0.001, Adonis, **Fig. 3a**). The non-phylogenetic Bray-Curtis dissimilarity analysis revealed a separation of the communities based on abundance of the five dominating *Bifidobacterium* species (*B. longum, B. bifidum, B. breve, B. catenulatum* group and *B. dentium*) (**Fig. 3b** and **Supplementary Fig. 12c-h**). Community abundance of *B. longum, B. bifidum* and *B. breve,* but not *B. catenulatum* group and *B. dentium* (**Fig. 3b**) matched the measured faecal concentrations of aromatic lactic acids (**Fig. 3c**). Consistently, faecal concentrations of ILA, PLA and 4-OH-PLA increased concurrently with an increase in absolute abundance of infant type *Bifidobacterium* species (defined as the summarized abundance of *B. longum, B. bifidum, B. breve* and *B. scardovii*) from birth to around 6 months of age (**Fig. 3d, upper panels**). The gut microbiota of individuals dominated by infant type *Bifidobacterium* spp. was more stable over time than in individuals with a gut microbiota not dominated by infant type *Bifidobacterium* spp. (p < 0.0001, Mann-Whitney *U* test) (**Supplementary Fig. 12i-j**). Using solely samples from breastfed infants, faecal abundances of HMO residuals showed a progressive decline with age, concurrent with the progressive increase in infant type *Bifidobacterium* species (**Fig. 3d, lower panels**). By repeated measure correlation analyses[28] (**Supplementary Fig. 13**) and partial Spearman's Rank correlation analyses[29] adjusted for age, we confirmed that the abundance of infant type *Bifidobacterium* species were positively associated with faecal levels of ILA, PLA and 4-OH-PLA and negatively associated with abundances of HMOs in faeces (**Fig. 3e**). Both subspecies of *B. longum* were associated with the aromatic lactic acids, but mainly *B. longum* subsp. *infantis* was associated with the HMO residuals in faeces (**Fig. 3e**). We have thus established a link between breastfeeding, degradation of HMOs, abundance of specific infant type *Bifidobacterium* spp. and concentrations of aromatic lactic acids in early infancy.

Examination of the *Bifidobacterium* and aromatic lactic acid dynamics in each of the 25 infants during the first 6 months of life (**Fig. 3f-h** and **Supplementary Fig. 14-15**) revealed that breastfed infants early colonised by infant type *Bifidobacterium* species consistently showed high concentrations of aromatic lactic acids in faeces (**Fig. 3f** and **Supplementary Fig. 15a,b**). In contrast, infants with delayed infant type *Bifidobacterium* species colonization showed considerably lower concentrations of the aromatic lactic acids, in particular of ILA, despite breastfeeding (**Fig. 3g** and **Supplementary Fig. 15c**). Among the latter, CIG08 and CIG09 were twins, born late preterm, and dominated by an OTU assigned to *Clostridium neonatale* (**Supplementary Fig. 11c** and **Supplementary Data 2b**) in accordance with previous reports on *C. neonatale* overgrowth[30] and delayed *Bifidobacterium* colonization[31–34] in preterm infants. CIG07 who also showed delayed colonization with infant type *Bifidobacterium*, was mixed fed throughout the whole period and predominantly colonised with *E. coli* and *Clostridium* spp. (**Supplementary Fig. 11c**). CIG18 had relatively low faecal concentrations of aromatic lactic acids until age 172 days, when *B. breve* replaced *B. dentium* (**Fig. 3g**), consistent with the fact that *B. dentium* lacks the *aldh* gene while *B. breve* contains it (**Fig. 2a,b**). Finally, in the three infants treated with antibiotics during our study, *Bifidobacterium* species abundance were temporarily decreased simultaneously with reduced concentrations of the aromatic lactic acids (**Fig. 3h**). This indicates that bifidobacterial aromatic lactic acid production is compromised by pre-term delivery, exposure to antibiotics and formula supplementation.

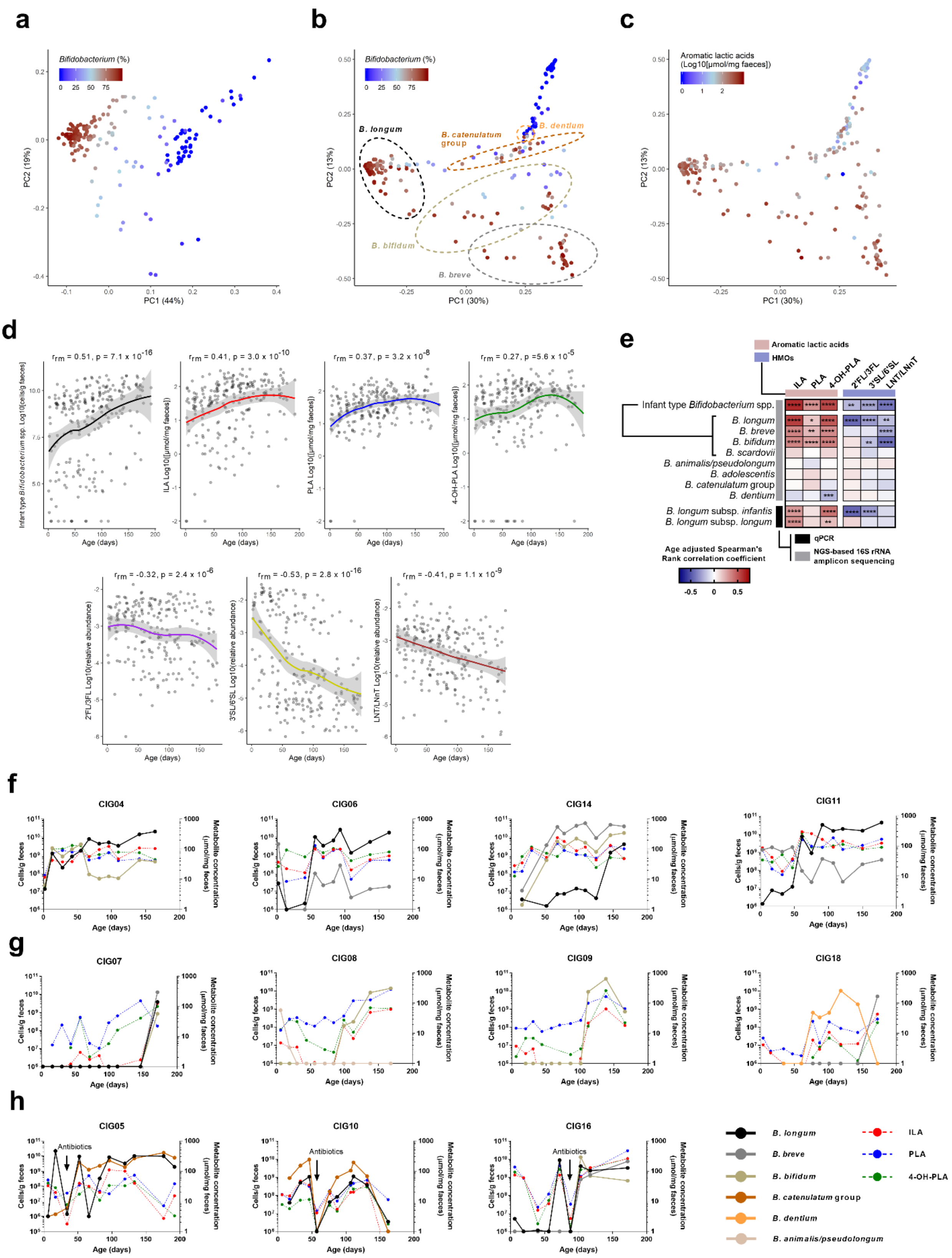

282

283

Fig. 3. Infant type *Bifidobacterium* species determine aromatic lactic acid concentrations during early infancy

a-c, Principal coordinate analysis plots of weighted UniFrac (a) or Bray-Curtis (b-c) distances/dissimilarities (n=234#), coloured according to relative abundance of *Bifidobacterium* (a-b) or $\log_{10}$ transformed absolute concentration [µmol/mg faeces] of aromatic lactic acids (sum of indolelactic acid (ILA), phenyllactic acid (PLA) and 4-hydroxyphenyllactic acid (4-OH-PLA)) in the Copenhagen Infant Gut (CIG) cohort. Dashed lined circles indicate communities dominated (relative abundance > 50%) either by *B. longum*, *B. bifidum*, *B. breve*, *B. catenulatum* group or *B. dentium* (*B. adolescentis*, *B. scardovii* and *B. animalis/pseudolongum* never dominated any of the communities, see **Supplementary Fig 11-12)**. #6 samples were omitted from the analyses due to low read counts (<8000).

d, Temporal development in absolute abundance of infant type *Bifidobacterium* spp. (defined as the sum of absolute abundances of *B. longum*, *B. breve*, *B. bifidum* and *B. scardovii*), faecal concentrations of aromatic lactic acids (ILA, PLA and 4-OH-PLA, n=240) and relative faecal abundance of HMOs (2'FL/3FL, 2'/3-*O*-fucosyllactose; 3'SL/6'SL, 3'/6'-*O*-sialyllactose; LNT/LNnT, lacto-N-tetraose/ lacto-N-*neo*tetraose, n=228) during the first 6 months of life in the CIG cohort. A local polynomial regression (LOESS) fit is shown with 95% CI shaded in grey. Statistical significance is evaluated by repeated measures correlations (r_{rm}).

e, Heatmap illustrating partial Spearman's Rank correlation coefficients (adjusted for age) between the absolute abundance of *Bifidobacterium* species/subspecies and absolute faecal concentrations of aromatic lactic acids (n=240) or relative abundances of HMOs (n=228) in the CIG cohort. Infant type *Bifidobacterium* spp. is the sum of absolute abundances of *B. longum*, *B. breve*, *B. bifidum* and *B. scardovii*. Statistical significance is indicated by asterisks with * p<0.05, **p<0.01, ***p<0.001 and ****p<0.0001.

f-h, Absolute abundance of *Bifidobacterium* spp. (>1% of total community) and concentrations of ILA, PLA and 4-OH-PLA in selected individuals from the CIG cohort. **f**, Fully breastfed infants and early colonised with high abundances of one or more of the infant *Bifidobacterium* spp. (*B. longum*, *B. breve* or *B. bifidum*) and concurrent high absolute concentrations of ILA, PLA and 4-OH-PLA through the first 6 months of life. **g**, Infants with delayed colonization of infant type *Bifidobacterium* spp. and concurrent low concentrations of ILA, PLA and 4-OH-PLA. **h**, Infants with recorded oral antibiotics intake during the first 6 months of life. Similar dynamics of the remaining infants can be seen in **Supplementary Fig. 15**.

See Supplementary Fig 11-15

Indolelactic acid is a relevant early life AhR agonist

The tryptophan-derived metabolite ILA was the most abundant aromatic lactic acid, as well as the most abundant tryptophan catabolite measured in the faeces of infants at 0-6 months (**Supplementary Table 2**) and 9 months of age (**Fig. 1d**). Microbial tryptophan catabolites have been found to contribute to intestinal and systemic homeostasis, in particular by their ability to bind the aryl hydrocarbon receptor (AhR)[12]. In accordance with previous reports[16,35], we observed modest but significant dose-dependent increases in agonistic activity of ILA in both rat and human AhR reporter gene cell lines (**Supplementary Fig. 16**). Notably, ILA was more potent in the human AhR compared to the rat AhR assay (**Supplementary Fig. 16**). To investigate the relationship between gut microbiota, aromatic amino acid metabolites and AhR signalling, the AhR activity induced by sterile-filtered faecal water from selected CIG infants (**Fig. 3f-h**) was associated to the most abundant bacterial taxa and all quantified aromatic amino acid metabolites (n=20) in the same samples (**Fig. 4a**).This revealed that particularly the infant type *Bifidobacterium* spp. were positively associated with AhR activity (**Fig. 4b & Supplementary Fig. 17a**). *B. dentium* also correlated positively with AhR activity despite the absence of an *aldh* gene in this species (**Fig. 4a**), which might be due to its association to the AhR agonist IAld (**Fig. 1e**), showing similar AhR reporter activity as ILA (**Supplementary Fig. 16a**). Of all the aromatic amino acid metabolites measured, only faecal concentrations of three known AhR agonists indoleacetic acid (IAA), IAld and in particular ILA were significantly associated with AhR activity (**Fig. 4a**,**c & Supplementary Fig. 17b**). Temporal development in AhR activity was assessed in the CIG samples, and stratification of infants into those colonised early (**Fig. 3f**) and late (**Fig. 3g**) with infant type *Bifidobacterium* spp. revealed a higher AhR activity of the faecal water of early colonised infants (**Fig. 4d-e**). These data show that ILA, produced by *Bifidobacterium* spp. of the infant gut, is a highly relevant AhR agonist in early life.

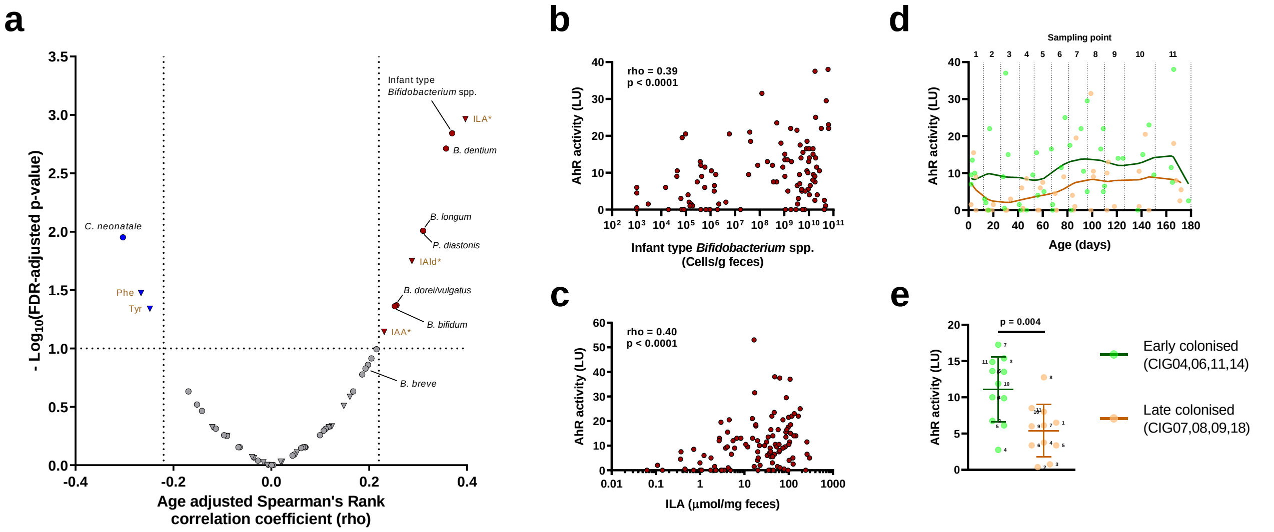

Fig. 4. Faecal concentrations of infant type *Bifidobacterium* spp. and indolelactic acid associate with AhR activity

a, Scatterplot of age adjusted Spearman's Rank correlation coefficients (versus associated FDR-adjusted p-values) between AhR activity (Luminescence Units, LU) of faecal water (n=119) from selected Copenhagen Infant Gut (CIG) infants (**Fig. 3f-h,** n=11) in a reporter cell line assay and absolute abundance of gut bacterial taxa (relative abundance>0.1%, n=40, circles) or quantities of aromatic amino acid catabolites (n=20, triangles) measured in the same samples. Coloured circles/triangles mark taxa/metabolites measures that are significantly positively (red) or negatively (blue) associated with AhR activity, within an FDR-adjusted p-value of 0.1. Labels are coloured brown for metabolites and black for bacterial taxa. Asterisks indicate known AhR agonists[16].

b-c, Scatterplots showing the associations from (a) between infant type *Bifidobacterium* spp. (b) or ILA (c) and AhR activity in faecal water from selected CIG infants, assessed by age adjusted Spearman's Rank correlation analysis.

d, Temporal development (11 samplings points) of *in vitro* AhR activity in CIG infants early (green; CIG04, CIG06, CIG11 and CIG14) or late (orange; CIG07, CIG08, CIG09, CIG18) colonised with infant type *Bifidobacterium* spp (See **Fig. 3f-g**). Locally weighted regression scatterplot smoothing (LOWESS) curves were fitted to the data points.

e, Scatterplots (mean ± SD) of AhR activity for each sampling point, stratifying samples into individuals early and late colonised with infant type *Bifidobacterium*. Statistical significance was evaluated by unpaired *t*-test.

See Supplementary Fig 16-17

DISCUSSION

The importance of intestinal commensal bacteria in regulation of the intestinal barrier function and immune development during infancy is well established[36,37]. Yet, specifically the symbiotic role of the breastmilk-promoted *Bifidobacterium* species, which are highly abundant in breastfed infants, remains largely unknown. Here we identified an aromatic lactate dehydrogenase, which catalyses the last step of the conversion of aromatic amino acids into their respective aromatic lactic acids in the infant gut. We show that only the infant type *Bifidobacterium* species contain the aromatic lactate dehydrogenase, explaining why *Bifidobacterium* species commonly isolated from the infant gut *in vitro* produce relative higher levels of ILA compared with other *Bifidobacterium* species[38]. The infant type *Bifidobacterium* species are adapted to breastfeeding by their HMO-transport and degradation genes, which provide them with a colonization advantage in infant gut[39–43]. Unlike HMO-utilization genes, the *aldh* gene appeared not to be important for bifidobacterial proliferation since disruption of the *aldh* gene did not compromise growth. However, acquisition of *aldh* genes in breastmilk-promoted *Bifidobacterium* species may provide an evolutionary advantage to the host. Here, our data suggest that the production of the AhR agonist ILA by breastmilk-promoted *Bifidobacterium* is a key determinant of AhR-dependent signalling in the gut during infancy. Indeed, our enzymatic assays show strong adaptation of ALDH towards indolepyruvate, resulting preferentially in the formation of ILA, the most abundant of the aromatic lactic acids and microbial tryptophan catabolites detected in our two cohorts. This is potentially of fundamental importance, since AhR signalling is essential for gut barrier function[44,45] and immune development[15,46–48]. Microbiota-produced tryptophan-derived AhR ligands (e.g. indolealdehyde) have been shown to confer colonization resistance against gastrointestinal pathogens[16], improve intestinal barrier function[44], attenuate induced colitis[49] and improve features of metabolic syndrome[44]. Further, although AhR is conserved across invertebrates and vertebrates, microbiota-derived tryptophan agonists have shown human-AhR selectivity[50]. In support of this, we found that ILA is a more potent ligand in the human compared to the rat AhR assay. Considering the strong dominance of ILA producing *Bifidobacterium* spp. in the gut of breastfed infants, we speculate that ILA provides an advantage to the infant host by contributing to AhR-mediated early life intestinal and metabolic homeostasis. A putative mechanism relates to the development of innate lymphoid cells (ILCs), which are important mediators of innate immunity to bacterial, viral and fungal infections[51]. A specific subset of ILCs, group 3 ILCs, shows AhR agonist dependency for survival and function and are reported to be crucial for resistance against gastrointestinal pathogens through the production of IL-22[16,48]. This effect has been shown to be mediated by microbiota-produced AhR-agonistic indoles[16]. Thus, we find it plausible that high levels of ILA produced by *Bifidobacterium* spp. in the infant gut contribute to innate protection against gastrointestinal pathogens. Further, AhR ligands (including ILA) have been shown to modulate the adaptive immune system by promoting IL-10+T_{reg} induction and suppressing IL-17 and IFNγ production by T-cells, potentially reducing the risk of autoimmunity[52–54]. Non-AhR mediated mechanisms may add to the protective effect, as ILA and PLA have been shown *in vitro* to have direct anti-bacterial[55,56] and anti-fungal properties[57,58]. Furthermore, ILA and PLA were recently identified as potent agonists of human hydroxycarboxylic acid receptor 3 (HCA3)[59], a receptor expressed in adipocytes, immune cells and in the intestinal epithelium[60], involved in the regulation of immune functions and energy homeostasis[61,62]. Thus, the production of aromatic lactic acids by human breastmilk-promoted *Bifidobacterium* during infancy may represent an evolutionary explanation as to why HCA3 is only expressed in humans and hominids[59]. In summary, the production of aromatic lactic acids via the newly identified aromatic lactate dehydrogenase found specifically in breastmilk-promoted species of *Bifidobacterium* might be an unprecedented feature contributing to intestinal homeostasis and immune development during infancy. These findings represent a major progress in the understanding of the beneficial effects of breastmilk, *Bifidobacterium* species and their metabolites for human health in early life.

METHODS

Human study populations and metadata

SKOT cohort

The discovery cohort consisted of a random subset of 59 healthy infants of the observational SKOT I cohort[19]. These infants were originally recruited from Copenhagen and Frederiksberg by random selection from the National Danish Civil Registry[63]. Inclusion criteria were single birth and full term delivery, absence of chronic illness and age of 9 months ± 2 weeks at inclusion. Mode of delivery, gender, age at sampling, use of medication, breast- and formula feeding prevalence as well as exclusive and total breastfeeding duration and age of introduction to solid foods was recorded by parental questionnaires (**Supplementary Data 1a,b**). Anthropometrics, full dietary assessment and other relevant metadata have been published previously[3,64]. Faecal samples were obtained at 9 months ± 2 weeks of age and were stored at -80°C until DNA extraction, as described previously[3]. Urine samples were collected by the use of cotton balls placed in the infants' disposable nappies from which the urine was squeezed into a sterile tube and stored at -80°C. In case of faeces in the nappy, the urine sample was discarded. The study protocol was approved by the Committees on Biomedical Research Ethics for the Capital Region of Denmark (H-KF-2007-0003) and The Data Protection Agency (2002-54-0938, 2007-54-026) approved the study. Informed consent was obtained from all parents of infants participating in the SKOT I study.

CIG cohort

The validation cohort, CIG, consisted of 25 healthy infants, vaginally born (23/25) and full-term (23/25) delivered. Infants in CIG were recruited through social media and limited to the Copenhagen region. Parents collected faecal samples approximately every second week, starting from the first week of life until 6 months of age (i.e. within week 0, 2, 4, 6, 8, 10, 12, 16, 20 and 24). Parents were instructed to collect faecal samples from nappies into sterile faeces collection tubes (Sarstedt, Nümbrecht, Germany) and immediately store them at -18°C in a home freezer until transportation to the Technical University of Denmark where the samples were stored at -80°C until sample preparation. Gender, pre-term vs full-term birth, mode of delivery, infant/maternal antibiotics, feeding patterns (breastmilk vs formula), introduction to solid foods and consumption of probiotics was recorded (**Supplementary Data 2a**). The Data Protection Agency (18/02459) approved the study. The office of the Committees on Biomedical Research Ethics for the Capital Region of Denmark confirmed that the CIG study was not notifiable according to the Act on

Research Ethics Review of Health Research Projects (Journal nr.: 16049041), as the study only concerned the faecal microbial composition and activity and not the health of the children. Informed consent was obtained from all parents of infants participating in the CIG study.

Gut microbiota analysis

16S rRNA gene amplicon sequencing

Sample preparation and sequencing was performed as previously described[3] using a subset of 59 faecal samples originating from infants participating in the SKOT I cohort and 241 faecal samples from 25 infants participating in the CIG cohort (data from a total of 28 samples were missing due to insufficient DNA extraction, lack of PCR product, very low number of sequencing reads or resemblance of community to negative controls). Briefly, DNA was extracted from 250 mg faeces (PowerLyzer® PowerSoil® DNA isolation kit, MoBio 12855-100) and the V3 region of the 16S rRNA gene was amplified (30s at 98°C, 24-30 cycles of 15s at 98°C and 30s at 72°C, followed by 5 min at 72°C) using non-degenerate universal barcoded primers[65] and then sequenced with the Ion OneTouch™ and Ion PGM platform with a 318-Chip v2. Sequences from SKOT and CIG were analyzed separately. Briefly, they were de-multiplexed according to barcode and trimmed as previously described[65,66] in CLC Genomic Workbench (v8.5. CLCbio, Qiagen, Aarhus, DK). Quality filtering (-fastq_filter, $MAX\_EE_{[SKOT]} = 2.0$, $MAX\_EE_{[CIG]} = 1.0$), dereplication, OTU clustering (-cluster_otus, minsize 4), chimera filtering (-uchime_ref, RDP_gold database), mapping of reads to OTUs (-usearch_global, id 97%) and generation of OTU tables (python, uc2otutab.py) was done according to the UPARSE pipeline[67]. In QIIME[68], OTU tables ($n_{OTUs[SKOT]} = 545$, $n_{OTUs[CIG]} = 478$) was filtered to include only OTUs with abundance across all samples above 0.005% of the total OTU counts ($n_{OTUs[SKOT]} = 258$, $n_{OTUs[CIG]} = 145$). OTU relative abundances within samples were estimated by total sum scaling. Taxonomy was assigned to the OTUs using the rdp classifier with confidence threshold 0.5[69] and the GreenGenes database v13.8[70]. Estimating species composition in the CIG cohort, the OTUs detected with identical taxonomy were collapsed and using a cutoff of average relative abundance of 0.1%, only 39 bacterial species/taxa remained, representing 97.5% of total community (**Supplementary Data 2b & Supplementary Fig. 11**). Based on PyNAST alignment of representative OTU sequences from each cohort separately, a phylogenetic tree was created with FastTree, as described previously[66]. Alpha diversity (Shannon index, Observed OTUs, Pielou's evenness index) and beta diversity (weighted and unweighted UniFrac distances, abundance weighted and binary Bray-Curtis and abundance weighted Jaccard dissimilarities) measures were calculated in QIIME, with the sequencing depth rarefied to 2,000 (SKOT) - 8,000 (CIG) sequences per sample. Jaccard similarity index (1- abundance weighted Jaccard distance) was computed by calculating the median of all Jaccard similarity index values between adjacent time points within each individual of the CIG cohort. In order to investigate *Bifidobacterium* species composition OTUs sequences classified as *Bifidobacterium* according to the GreenGenes database v13.8 were filtered to remove low abundant OTUs (cutoff 0.1% of total *Bifidobacterium*) and the taxonomy of these resulting OTUs ($n_{OTUs[SKOT]} = 23$, $n_{OTUs[CIG]} = 8$) was confirmed by BLAST[71] search against the 16S rRNA gene sequence database at NCBI. The top BLAST hit indicated species annotation (**Supplementary Data 1f and 2c**). OTUs were collapsed into *Bifidobacterium* species (*B. longum, B. bifidum, B. breve, B. catenulatum* group, *B. adolescentis, B. scardovii, B. dentium, B. animalis/pseudolongum)* based on the top BLAST hit (**Supplementary Data 1f and 2c**).

Quantitative PCR

Total bacterial load (universal primers) and absolute abundances of *B. longum* subsp. *longum* and *B. longum* subsp. *infantis* (subspecies specific primers) were estimated by quantitative PCR (qPCR), using the primers listed in **Supplementary Table 3**. Each reaction was performed (in triplicates) with 5 µl PCR-grade water, 1.5 µl forward and reverse primer, 10 µl SYBR Green I Master 2X (LightCycler® 480 SYBR Green I Master, Roche) and 2 µl template DNA, in a total volume of 20 µl. Standard curves were generated from 10-fold serial dilutions of linearized plasmid (containing 10^8-10^0 gene copies/µl), constructed by cloning a PCR amplified 199bp fragment of the 16S rRNA gene (V3-region) of *E. coli* (ATCC 25922) or a 307bp fragment of the Blon0915 gene[72] of *B. longum* subsp. *infantis* (DSM 20088) or a 301bp fragment of the BL0274 gene[73] of *B. longum* subsp. *longum* (DSM 20219) into a pCR4-Blunt-TOPO (Invitrogen) or pCRII-Blunt-TOPO vector (Invitrogen). Plates were run on the LightCycler® 480 Instrument II (Roche) with the program including 5 min pre-incubation at 95°C, followed by 45 cycles with 10 sec at 95°C, 15 sec at 50-60°C and 15 sec at 72°C and a subsequent melting curve analysis including 5 min at 95°C, 1 min at 65°C and continuous temperature increase (ramp rate 0.11 °C/s) until 98°C. Data were analyzed with the LightCycler® 480 Software (v1.5) (Roche). Bacterial load data (using the universal primers) were used to estimate absolute abundances of each microbial taxa by multiplying with relative abundances (derived from 16S rRNA gene amplicon sequencing).

Bifidobacterium strains and growth experiments

Aromatic lactic acid production by Bifidobacterium type strains

Bifidobacterium type strains (**Supplementary Table 4**) were cultivated on MRSc (MRS containing 2% (w/v) glucose and supplemented with 0.05% (w/v) L-cysteine) agar plates for 48h at 37°C anaerobically. Single colonies were dissolved in 5.0 mL pre-reduced MRSc broth and incubated for 24h at 37°C anaerobically with shake. The overnight cultures were washed (10000xg, room temperature, 5 min) and resuspended in sterile 0.9% NaCl water, diluted 1:20 (in triplicates) in pre-reduced MRSc or MRSc+HMOs (MRS broth without glucose, but supplemented with 2.0% (w/v) HMO mixture and 0.05% (w/v) L-cysteine) and re-incubated at 37°C anaerobically for 72h, after which OD_{600nm} was measured and the culture supernatants (16000xg, 5 min, 4°C) were analysed by UPLC-MS. The individual HMOs were kindly donated by Glycom A/S (Hørsholm, Denmark); 2'-*O*-fucosyllactose (2'FL), 3-*O*-fucosyllactose (3FL), lacto-*N*-tetraose (LNT), lacto-*N*-*neo*tetraose (LN*n*T), 6'-*O*-sialyllactose (6'SL), 3'-*O*-sialyllactose (3'SL), together representing the three structures found in human breastmilk (fucosylated, sialylated, and neutral core). Based on the HMO composition in breastmilk[74,75], these were mixed in a ratio of 53% 2'FL, 18% 3FL, 13% LNT, 5% LN*n*T, 7% 6'SL and 4% 3'SL in sterile water to obtain a representative HMO mix used in the *in vitro* experiments at 2% (w/v).

Growth experiment with B. longum* subsp. *longum 105-A strains

B. longum subsp. *longum* 105-A (JCM 31944) was obtained from Japan Collection of Microorganisms (RIKEN BioResource Research Center, Tsukuba, Japan). *B. longum* subsp. *longum* 105-A strains (wild type [WT], insertional mutant [type4 *ldh*::pMSK127] and complemented insertional mutant [type 4 *ldh*::pMSK127 / pMSK128 (P*xfp*-type4 *ldh*)]; **Supplementary Table 4**) were cultivated on MRSc or MRSc-Chl (MRSc supplemented with 2.5 μg/mL chloramphenicol) agar plates for 48h at 37°C anaerobically. Single colonies were dissolved in 5.4 mL MRSc or MRSc-Chl broth, 10-fold serially diluted and incubated for 15h at 37°C anaerobically with shake. The most diluted culture (exponential phase) was washed in same medium (10000xg, room temperature, 5 min) and resuspended in MRSc or MRSc-Chl broth to yield OD_{600nm} = 1 and subsequently diluted 1:40 in prewarmed and reduced MRSc or MRSc-Chl broth (in triplicates), before incubation at 37°C, anaerobically with shake. The cultures were sampled (500 μL) every hour for OD_{600nm} measurements and the culture supernatants (16000xg, 4°C, 5 min) from early (13h) stationary phase was analyzed by UPLC-MS for aromatic amino metabolites and by GC-MS for lactate.

Alignments and construction of phylogenetic trees

From the full genome sequences (available at https://www.ncbi.nlm.nih.gov/genome/) of *Bifidobacterium* type strains included in this study (**Supplementary Table 4**) all genes annotated as L-lactate dehydrogenases were aligned (gap cost 10, gap extension cost 1) and subsequently a phylogenetic tree (Algorithm = Neighbor-Joining, Distance measure = Jukes-Cantor, 100 bootstrap replications) was constructed in CLC Main Workbench (v7.6.3, CLCbio, Qiagen, Aarhus, DK). The tree was visualized by use of the FigTree software v1.4.3 (http://tree.bio.ed.ac.uk/software/figtree/). In addition, the type 4 LDH amino acid sequence (translated from the type 4 ldh nucleotide sequence) of *B. longum* subsp. *longum* 105-A was aligned (gap cost 10, gap extension cost 1) with the type 4 LDH amino acid sequences of the *B. longum* subsp. *longum*, *B. longum* subsp. *infantis*, *B. bifidum*, *B. breve* and *B. scardovii* type strains. Comparison of type 4 *ldh* gene cluster/operon in 12 *Bifidobacterium* type strains (**Supplementary Fig. 5**) was basically conducted by pairwise alignments in MBGD (Microbial Genome Database for Comparative Analysis; http://mbgd.genome.ad.jp/). The amino acid sequences of the gene cluster from *B. pseudolongum* subsp. *pseudolongum* type strain was collected from NCBI database (https://www.ncbi.nlm.nih.gov/genome/) and was used for comparison with that from *B. animalis* subsp. *animalis* type strain.

Recombinant expression of type 4 *ldh*

Chemically competent cells for recombinant expression

E. coli LMG 194 ON culture (200μL) was inoculated into 5 ml Luria-Bertani (LB) medium and incubated at 37°C, 250 rpm until OD_{600nm} = 0.5, at which the culture was centrifuged 5 min at 10000xg at 4°C and supernatant discarded. Cell pellet was resuspended in ice-cold 1.8 ml 10mM $MgSO_4$ (Sigma, M2643) and centrifuged for 2 min at 5000xg at 0°C. Supernatant was discarded and cell pellet resuspended in 1.8 ml ice-cold 50 mM $CaCL_2$ (Merck, 1.02083.0250), incubated on ice for 20 min and centrifuged for 2 min at 5000xg at 0°C. Cell pellet was resuspended in 0.2 ml ice-cold 100mM $CaCl_2$, 10mM $MgSO_4$ and placed on ice until transformation.

Cloning and recombinant expression

Genomic DNA was extracted (PowerLyzer® PowerSoil® DNA isolation kit, MoBio 12855-100) from colony material of *B. longum* subsp. *infantis* DSM 20088^T. In order to amplify the type 4 *ldh* gene, 50 ng template DNA was mixed with 5 µL 10X PCR buffer, 0.5 µL (50 mM) dNTP mix, 1 µL (10µM) forward primer (ldh4_F, 5'-ACCATGGTCACTATGAACCG-3'), 1 µL (10µM) reverse primer (ldh4_R, 5'-AATCACAGCAGCCCCTTG-3') and 1 µL (1 U/µL) Platinum Taq DNA polymerase (Invitrogen, 10966-018) in a 50 µL total reaction volume. The PCR program included 2 min at 94°C, 35 cycles of 30 sec at 94°C, 30 sec at 55°C, 60 sec at 72°C, followed by a final extension 10 min at 72°C. The PCR product was purified (MinElute PCR purification kit, Qiagen, 28004) and 4 µL was mixed with 1 µL Salt solution (1.2M NaCl, 0.06M $MgCl_2$) and 1 µL pBAD-TOPO® plasmid (Invitrogen, K4300-01) and incubated for 5 minutes at room temperature. 2 µL of the cloning mixture was transformed into 50 µL One Shot® TOP10 Competent Cells (Invitrogen, K4300-01) by gentle mix, incubation 15 min on ice and heat-shock for 30 sec at 42°C. 250µL S.O.C medium (Invitrogen, K4300-01) was added and incubated at 37°C for 1 h at 200 rpm and subsequently spread on LB-AMP (LB supplemented with 20 µg/ml Ampicillin (Sigma, A9518)) agar plates and incubated at 37°C ON. Transformants were picked and clean streaked on LB-AMP agar plates, incubated 37°C, ON and afterwards single colonies of each transformant was inoculated into 5 ml LB-AMP broth and incubated at 37°C for 15 h at 250 rpm. Plasmid DNA was isolated (QIAprep Spin Miniprep Kit, Qiagen, 27104) from each transformant and subsequently 5 µL plasmid DNA (80-100 ng/µL) was mixed with 5µL (5pmol/µL) pBAD forward (5'-ATGCCATAGCATTTTTATCC-3') or reverse (5'-GATTTAATCTGTATCAGG-3') sequencing primers (5pmol/µL) and shipped for sequencing at GATC (GATC-biotech, Koln, Germany). In order to remove the leader peptide in pBAD-TOPO, 10 µL plasmid (0.1 µg) with correct insert was cut with FastDigest *NcoI* (Thermo Scientific, FD0563) for 10 min at 37°C and the enzyme inactivated 15 min at 65°C. Plasmid was ligated using 1 µL (1U/µL) T4 DNA Ligase (Invitrogen, 15224-017) for 5 min at room temperature and subsequently 2µl plasmid was transformed into 100µl chemically competent *E. coli* LMG194 cells by incubation on ice for 30 min, followed by heat-shock at 43°C for 3 min and incubation on ice for 2 min. 900µL LB medium was added and cells were incubated at 37°C for 1h at 250 rpm, before plating on LB-AMP agar plates and incubation at 37°C ON. Transformants were picked, clean streaked and plasmid DNA isolated and sequenced as described above. A transformant with correct insert was selected for recombinant expression of the type 4 *ldh* gene; 2 ml LB-AMP broth was inoculated with a single recombinant colony or the non-transformed *E. coli* LMG194 (negative control) and grown at 37°C ON at 250rpm. In 3x triplicates, 100 µL of the ON cultures (2x3x 100 µL transformant culture + 1x3x 100 µL non-transformed *E. coli* LMG194 culture) were diluted 100-fold into 9.9 mL prewarmed LB-AMP/LB broth and grown at 37°C, 250 rpm until $OD_{600nm} \approx 0.5$, at which 9 mL culture was added 1 mL mix of indolepyruvic acid, phenylpyruvic acid and 4-hydroxyphenylpyruvic acid (1mg/mL each). The cultures were sampled (time zero) and subsequently 100 µL 20% L-arabinose (or 100 uL sterile water; control for induction) was added to induce gene expression and the cultures were re-incubated at 37°C, 250 rpm, before sampling at 1 h and 5 h post-induction for OD_{600nm} measurements and assessment of production of aromatic lactic acids. For the latter, samples were centrifuged at 16000xg, 5 min, 4°C and supernatants were stored at –20°C for UPLC-MS analyses.

Construction of type 4 *ldh* insertional mutant

Transformation of B. longum subsp. *longum 105-A*

B. longum subsp. *longum* 105-A cells were grown to exponential phase at 37°C in Gifu anaerobic liquid medium (Nissui Pharmaceutical Co., Ltd., Tokyo, catalog no. 05422), harvested by centrifugation, and washed twice with ice-cold 1 mM ammonium citrate buffer containing 50 mM sucrose (pH = 6.0). The cells were concentrated 200 times with the same buffer and used for electroporation with settings of 10 kV/cm, 25 µF, and 200Ω. After recovery culturing in Gifu anaerobic liquid medium at 37°C for 3 h, the cells were spread onto Gifu anaerobic agar containing antibiotics (i.e. 30 µg/mL spectinomycin and/or 2.5µg/mL chloramphenicol) for selection.

Insertional mutant construction and plasmid complementation

The type 4 *ldh* gene (BL105A_0985) of *B. longum* subsp. *longum* 105-A was disrupted by a plasmid-mediated single crossover event as described previously[76]. The plasmid used for disruption was constructed using the In-Fusion cloning kit (Clontech Laboratories, Inc., Mountain View, CA, USA, catalog no. 639649). *Escherichia coli* DH5α was used as a host. In brief, the internal region of the *ldh* gene (position 142-638 of the nucleotide sequence of BL105A_0985, see **Supplementary Fig. 6**) was amplified by PCR using a primer pair Pr-580/581 (**Supplementary Table 5**) and ligated with the BamHI-digested pBS423 fragment carrying pUC *ori* and a spectinomycin resistance gene[26]. The resulting plasmid pMSK127 was introduced into *B. longum* subsp. *longum* 105-A by electroporation to be integrated into type 4 *ldh* locus by single crossover recombination (type 4 *ldh*::pMSK127). Type 4 *ldh* disruption was confirmed by PCR with a primer pair designed to anneal outside of the gene (**Supplementary Fig. 6** and **Supplementary Table 5**). The amplified fragment was also sequenced to ensure the correct recombination event. Complementation plasmid pMSK128 was constructed by ligating PCR-amplified *xfp* (xylulose 5-phosphate/fructose 6-phosphate phosphoketolase) promoter region (P*xfp*) and the type 4 *ldh* coding region with PstI- and SalI-digested pBFS38[77] using the In-Fusion cloning kit, by which type 4 *ldh* was placed under the control of P*xfp*. Primer pairs of Pr-598/Pr-599 and Pr-600/Pr-601 were used for amplifying P*xfp* from pBFS48[77] and the type 4 *ldh* gene from the *B. longum* subsp. *longum* 105-A genome, respectively (**Supplementary Table 5**). The resulting plasmid was electroporated into type 4 *ldh*::pMSK127 to give type 4 *ldh*::pMSK127 / pMSK128 (P*xfp*-type4_*ldh*) (**Supplementary Fig. 6**).

Biochemical characterization of type 4 LDH

Recombinant expression and purification

Type 4 LDH (BL105A_0985) was recombinantly expressed as a non-tagged form. The gene was amplified by PCR using the genomic DNA of *B. longum* subsp. *longum* 105-A as a template and a primer pair of Pr-617 (5'-GGTGGTGGTGCTCGAGTCACAGCAGCCCCTCGCAG-3') and Pr-635 (5'-AAGGAGATATACATATGGTCACTATGAACCGC-3'). Underlined bases indicate 15-bp for In-Fusion cloning (Clontech). The amplified DNA fragment was inserted into the NdeI and XhoI site of pET23b(+) (Novagen) using an In-Fusion HD cloning kit (Clontech). The resulting plasmid was introduced into *E. coli* BL21 (DE3) Δ*lacZ* carrying pRARE2[76], and the transformant was cultured in LB medium supplemented with ampicillin (100 μg ml^{-1}) and chloramphenicol (7.5 μg ml^{-1}). When OD_{600nm} reached 0.5, isopropyl β-D-thiogalactopyranoside was added at a final concentration of 0.02 mM to induce the protein expression. The culture was incubated for four days at 18°C, harvested by centrifugation, and resuspended in 50 mM potassium phosphate buffer (KPB; pH 7.0) supplemented with 1 mM 2-mercaptoethanol (2-ME) and 200 μM phenylmethane sulfonyl fluoride. Following cell disruption by sonication, the cleared lysate was saturated with ammonium sulfate (40–60%). The resulting precipitate was dissolved, dialyzed against 20 mM KPB (pH 7.0) containing 1 mM 2-ME, and concentrated by Amicon Ultra 10K centrifugal device (Merck Millipore). The sample was then loaded onto an Affigel blue column (Bio-Rad) preequilibrated with 20 mM KPB (pH 7.0) containing 1 mM 2-ME, and eluted by the same buffer containing 1 M NaCl. The protein was further purified by a Mono Q 5/50 (GE Healthcare; a linear gradient of 0–1 M NaCl in 20 mM Tris-HCl (pH 8.0) containing 1 mM 2-ME) and Superdex 200 Increase 10/300 GL column (GE Healthcare; 10 mM KPB [pH 7.0] containing 50 mM NaCl and 1 mM 2-ME). Protein concentration was determined by measuring the absorbance at 280 nm based on a theoretical extinction coefficient of 26,470 M^{-1} cm^{-1}.

Enzyme assay

The standard reaction mixture contained 100 mM KPB (pH 8.0), 1 mM 2-ME, 0.1 mM β-NADH, and the substrate. The reaction was initiated by adding the enzyme, and the mixture was incubated at 37°C for an appropriate time, in which the linearity of the reaction rate was observed. The substrate concentrations were varied between 0.01 and 0.25 mM for IPA, 1.5 and 12.75 mM for PPA, 2 and 24 mM for 4-OH-PPA, and 2.5 and 40 mM for pyruvic acid. The enzyme was used at the concentrations of 0.22 nM for IPA, 1.47 nM for PPA, 0.12 nM for 4-OH-PPA, and 88.50 nM for pyruvic acid. The reducing reactions of PPA and pyruvic acid was continuously monitored by measuring the decrease of the absorbance at 340 nm (NADH consumption). When 4-OH-PPA and IPA were used as the substrates, the reaction products 4-OH-PLA and ILA were quantified by HPLC after the termination of the reactions by adding 5 % (w/v) trichloroacetic acid. HPLC analysis was performed using a Waters e2695 separation module (Waters) equipped with a LiChrospher 100 RP-18 column (250 × 4 mm, φ = 5 μm; Merck Millipore) at 50°C. Following equilibration with a mixture of 10% solvent A (50% methanol, 0.05% trifluoroacetic acid) and 90% solvent B (0.05% trifluoroacetic acid) at a flow rate of 1 mL/min, the concentration of solvent A was linearly increased to 100 % for 25 min and maintained at 100 % for additional 15 min. 4-OH-

PLA and ILA were detected by a Waters 2475 Fluorescence Detector with λ_{ex} 277 nm and λ_{em} 301 nm and λ_{ex} 282 nm and λ_{em} 349 nm, respectively. The standard curves were created using the known concentrations of both compounds. The kinetic parameters (k_{cat}, $K_{0.5}$, and Hill coefficient n_H) were calculated by curve-fitting the experimental data to the Hill equation, using KaleidaGraph version 4.1 (Synergy Software). Experiments were performed at least in duplicate. Physicochemical property of the enzyme was examined by using 1 mM PPA as a substrate. The effects of metal ions (0.1 mM each) on the enzyme activity was examined using 50 mM MES (2-(*N*-morpholino)ethanesulfonic acid) buffer (pH 7.0). EDTA (ethylenediaminetetraacetic acid) was added at the final concentration of 0.1, 0.5, or 1 mM. The optimal pH was determined using 50 mM KPB (pH 6.0–8.5) and TAPS (*N*-Tris(hydroxymethyl)methyl-3-aminopropanesulfonic acid) buffer (pH 8.0–9.0). The thermostability was evaluated by the residual activities after incubating the enzyme (1.0 mg/ml in 10 mM KPB [pH 7.0] containing 50 mM NaCl and 1 mM 2-ME) at the indicated temperatures for 30 min prior to the assay. Fructose-1,6-bisphosphate, shikimate-3-phosphate, D-erythrose-4-phosphate, and phosphoenolpyruvate were added to the reaction mixtures at the concentrations of 0.1 and 1 mM to examine their heterotropic effects. KPB, TAPS buffer, or HEPES (4-(2-hydroxyethyl)-1-piperazineethanesulfonic acid) buffer (pH 8.0 each) containing 1 and 4 mM PPA as a substrate was used. The effect of phosphate ion was analyzed by adding various concentration of KPB (pH 8.0) into 10 mM HEPES buffer (pH 8.0). All experiments were conducted at least in duplicate. In the subsequent kinetic analysis, we used phosphate ion at the concentration of 100 mM because (i) no saturation was obtained for phosphate under the tested conditions (**Supplementary Fig. 10a**), (ii) the intracellular phosphate concentration in Gram-positive bacteria is known to be 130 mM at maximum[78], and (iii) the strong homotrophic effect of the substrate PPA was observed only in the presence of 10 mM phosphate ion.

Metabolomics

Chemicals

Authentic standards of the aromatic amino acids and derivatives (**Supplementary Table 1**) were obtained from Sigma Aldrich (Germany), whereas isotope-labelled aromatic amino acids used as internal standards (L-Phenylalanine (ring-d5, 98%), L-Tyrosine (ring-d4, 98%), L-Tryptophan (indole-d5, 98%) and indoleacetic acid (2,2-d2, 96%)) of the highest purity grade available were obtained from Cambridge Isotope Laboratories Inc. (Andover, MA).

Extraction of metabolites from faecal samples

Faecal samples (100-500 mg) were diluted 1:2 with sterile MQ water, vortexed for 10 seconds and centrifuged at 16.000xg, 4°C for 5 minutes. Subsequently, the supernatant liquor was transferred to a new tube and centrifuged again at 16.000xg, 4°C for 10 minutes. Finally, an aliquot of 150-300 µL was stored at -20°C. All samples were later thawed at 4°C, centrifuged at 16.000xg, 4°C for 5 minutes, and diluted in a total volume of 80 µL water corresponding to a 1:5 dilution of the faecal sample. To each sample, 20 µL internal standard mix (4 µg/mL) and 240 µL of acetonitrile were added. The tubes were vortexed for 10 seconds and left at -20°C for 10 minutes to precipitate the proteins. The tubes were then centrifuged at 16.000xg, 4°C for 10 minutes and each supernatant

(320 µL) was transferred to a new tube, which was dried with nitrogen gas. Subsequently, the residues were reconstituted in 80 µL water (equalling a 1:5 dilution of the faecal sample with internal standards having a concentration of 1 µg/mL), vortexed for 10 seconds, centrifuged at 16.000xg, 4°C for 5 minutes, and transferred to LC vial, which was stored at -20°C until analysis.

Extraction of metabolites from urine samples

Urine samples (n=49) from the SKOT cohort were thawed in a refrigerator and all procedures during the sample preparation were carried out at 0-4°C using an ice bath. The subjects were randomized between analytical batches by placing all the samples from the each subject in the same 96 well-plate. The run order of the samples was randomized within the analytical batch. Urine samples were centrifuged at 3000xg for 2 minutes at 4°C. 150 µL of each urine sample were added to separate wells and diluted with 150 µL of diluent (MQ water: Formic acid (99.9:0.1, v/v) / Internal standard mixture (100 µg/mL) (90:10, v/v). A blank sample (diluent), standard mixture of external standard containing 44 biologically relevant metabolites (metabolomics standard)[79] and pooled sample containing equal amount of each sample (20 µL) were added to spare wells as quality control samples. The plates were stored at -80°C until the analysis. Immediately prior to analysis, the plates were thawed and mixed by vortex stirring for 10 minutes.

Extraction of metabolites from in vitro fermentation samples

Supernatants from *in vitro* fermentations were thawed at 4°C, centrifuged at 16.000xg, 4°C for 10 minutes, before 80 µL was transferred to a new tube. To each sample, 20 µL internal standard (40 µg/mL) and 300 µL of acetonitrile were added. The tubes were vortexed for 10 seconds and left at -20°C for 10 minutes to precipitate the proteins. Following, the tubes were centrifuged at 16.000xg, 4°C for 10 minutes before 50 µL of each sample was diluted with 50 µL of sterile water and transferred to a LC vial (equalling a 1:10 dilution of the sample with internal standards having a concentration of 1 µg/mL).

Metabolic profiling of faecal and in vitro samples using UPLC-MS

Aromatic amino acids and derivatives (**Supplementary Table 1**) of faecal and *in vitro* samples were quantified by ultra performance liquid chromatography mass spectrometry (UPLC-MS) as previously published[80].

In brief, samples were analysed in random order. For the analysis of the CIG faecal samples, a pooled quality control (QC) sample was injected for every 10 sample. In all cases, five standard mix solutions (0.1 µg/mL, 0.5 µg/mL, 1 µg/mL, 2 µg/mL and 4 µg/mL) were analysed once for every 10 samples to obtain a standard curve for every 10 samples. For each sample, a volume of 2 µL was injected into a ultra-performance liquid chromatography quadrupole time-of-flight mass spectrometry (UPLC-QTOF-MS) system consisting of Dionex Ultimate 3000 RS liquid chromatograph (Thermo Scientific, CA, USA) coupled to a Bruker maXis time of flight mass spectrometer equipped with an electrospray interphase (Bruker Daltonics, Bremen, Germany) operating in positive mode. The analytes were separated on a Poroshell 120 SB-C18 column with a dimension of 2.1x100 mm and 2.7 µm particle size (Agilent Technologies, CA, USA) as previously published[80]. Aromatic amino acids and derivatives were detected by selected ions and quantified by isotopic internal standards with similar molecular structures as listed in **Supplementary Table 1**. Data were processed using QuantAnalysis version 2.2 (Bruker Daltonics, Bremen, Germany) and bracket calibration curves for every 10 lumen samples were obtained for each metabolite. The calibration curves were established by plotting the peak area ratios of all of the analytes with respect to the internal standard against the concentrations of the calibration standards. The calibration curves were fitted to a quadratic regression.

For untargeted metabolomics, the raw UPLC-MS data, obtained by analysis of the CIG faecal samples in positive ionization mode, were converted to mzXML files using Bruker Compass DataAnalysis 4.2 software (Bruker Daltonics) and pre-processed as previously reported[81] using the R packpage XCMS (v.1.38.0)[82]. Noise filtering settings included that features should be detected in minimum 50% of the samples. A data table was generated comprising mass-to charge (*m/z*), retention time and intensity (peak area) for each feature in the every sample. The data were normalized to the total intensity. Subsequently, features with a coefficient of variation above 0.3 in the QC samples and features with a retention time below 0.5 min were excluded from the data. Parent ion masses of compounds of interest (2'FL/3FL, LNT/LN*n*T, 3'SL/6'SL) were searched in the cleaned dataset with 0.02 Da *m/z* and 0.02 min retention time tolerance. Subsequently, the identities of the features of interest were confirmed at level 1[83] by tandem mass spectrometry and comparison to authentic standards (**Supplementary Table 6**). Of notice, HMO isomers could not be distinguished with the method applied due to identical retention times.

Metabolic profiling of urine samples using UPLC-MS

The samples were analysed by UPLC coupled with a quadrupole-Time of Flight Mass Spectrometer (q-TOF-MS) equipped with an electrospray ionization (ESI) (Waters Corporation, Manchester, UK). Reverse phase HSS T3 C_{18} column (2.1x100 mm, 1.8 µm) coupled with a pre-column (VanGuard HSS T3 C18 column (2.1x5 mm, 1.8 µm)) were used for chromatographic separation. Five µl of each well was injected into the mobile phase A (0.1 % formic acid in MQ water), mobile phase B (10% 1M ammonium acetate in methanol), mobile phase C (methanol) and mobile phase D (isopropanol). Mobile phase gradient during the run time of 10 min was as follows: start condition (100 % A), 0.75 min (100 % A), 6 min (100 % C), 6.5 min (70 % B, 30 % D), 8 min (70 % B, 30 % D), 8.1 min (70 % B, 30 % D), 9 min (100 % A), 10 min (100 % A). The flow rate gradient was as follows: start condition (0.4 mL/min), 0.75 min (0.4 mL/min), 6 min (0.5 mL/min), 6.5 min (0.5 mL/min), 8 min (0.6 mL/min), 8.10 min (0.4 mL/min), 9 min (0.4 mL/min), 10 min (0.4 mL/min). ESI was operated in negative mode with 3.0 kV capillary probe voltage. The cone voltage and the collision energy were set at 30 kV and 5 eV, respectively. Ion source and desolvation gas (nitrogen) temperature were 120 and 400 ^{o}C while sampling cone and desolvation gas flow rates were 50 and 1000 l/hr. Scan time set as 0.08 s with 0.02 sec interscan time for both modes. Data were acquired in centroid mode with mass range between 50 to 1500 Da. Leucine-enkephalin (500 ng/ml) was infused as the lock-spray agent to calibrate the mass accuracy every 5 sec with 1 sec scan time. Quality control samples were used to evaluate possible contamination, monitoring the changes in mass accuracy, retention time and instrumental sensitivity drifts[79,84].

The raw data were converted to netCDF format using DataBridge Software (Waters, Manchester, UK) and imported into MZmine version 2.28[85]. A subset of samples was used to optimize the pre-processing parameters for the positive and negative mode data separately. Optimized pre-processing parameters are listed in **Supplementary Table 7**. Data pre-processing was employed with the following steps: mass detection, chromatogram builder, chromatogram deconvolution, deisotoping, peak alignment and gap filling. After the pre-processing, each detected peak was represented by a feature defined with a retention time, *m/z* and peak area.

The data matrix was imported into MATLAB R2015b (The MathWorksInc., Natick, MA). Features that were present in the blanks, were very early and late eluting (rt<0.30 and rt>9.46 min), potential isotopes, duplicates as well as features with masses indicating multiple charges were removed from the dataset using an in-house algorithm. The data were normalized using unit length normalization to correct the variation in urine concentration. Parent ion masses of the aromatic lactic acids (ILA, PLA and 4-OH-PLA) were searched in the cleaned dataset with 0.02 Da *m/z* and 0.02 s retention time tolerance. A linear regression model were employed feature wise to correct for batch differences and instrumental sensitivity drifts[86]. The aromatic lactic acids were confirmed at level 1[83] by comparison to authentic standards and by tandem mass spectrometry using the same experimental conditions (**Supplementary Fig. 2-4**).

Lactate production by B. longum* subsp. *longum 105-A strains using GC-MS

The lactate production of the *B. longum* subsp. *longum* 105-A wild-type, type 4 *ldh* mutant and type 4 *ldh* complemented strains were assessed in supernatants obtained after 13h of growth (early stationary phase) by gas-chromatography mass spectrometry (GC-MS) upon methyl chloroformate (MCF) derivatisation using a slightly modified version of the protocol previously described[87]. All samples were analysed in a randomized order. Analysis was performed using GC (7890B, Agilent Technologies, Inc., Santa Clara, CA) coupled with a quadrupole detector (59977B, Agilent Technologies, Inc., Santa Clara, CA). The system was controlled by ChemStation (Agilent Technologies, Inc., Santa Clara, CA). Raw data was converted to netCDF format using Chemstation, before the data was imported and processed in Matlab R2014b (Mathworks, Inc.) using the PARADISe software[88].

Rat Aryl hydrocarbon receptor (AhR) reporter gene assay

Stably transfected rat hepatoma (H4IIE-CALUX) cells provided by Dr. Michael Denison (University of California, USA) were used. The assay was conducted as previously described[89], where cells were incubated for ~22 h in Minimum Essential Medium (MEM)α with 1% foetal bovine serum (FBS) and 1% penicillin/streptomycin/fungizone. Chemical exposure was performed for 24 h, and successively luminescence was measured. Cell viability was analyzed by measuring ATP levels with the CellTiter-Glo® Luminescense Assay according to the manufacturer's instruction (Promega, Denmark). 2,3,7,8-Tetrachlorodibenzo-p-dioxin (TCDD) was used as a positive control. Three experiments in triplicates were conducted with five 2-fold dilutions of ILA and IAld ranging from 12.5 to 200 µM with a constant vehicle concentration in all wells. Further, sterile filtered fecal water (10 mg faeces/ml MQ water) obtained from all samples (n=119) of 11 selected CIG infants (**Fig. 3f-h**) were run in technical triplicates in the assay. Only mild toxicity that did not correlate with AhR-luminesence signal was observed for some fecal water samples.

Human AhR reporter gene assay

ILA and IAld (positive control)[16] were tested for activation of the human AhR. AhR Reporter Cells from Indigo Biosciences (PA, USA) that include the luciferase reporter gene functionally linked to an AhR-responsive promoter were used. The assay was run according to the instructions of the manufacturer (technical manual version 6.0) with the reference agonist MeBIO as the positive control. Three experiments in triplicates were conducted with five 2-fold dilutions of ILA and IAld ranging from 12.5 to 200 µM with a constant vehicle concentration in all wells. No cytotoxicity was observed for any of the tests as determined by a resazurin toxicity assay.

Statistical analyses

Statistical analyses were performed using QIIME v1.9[68], R v3.1[90] and GraphPad Prism v8.1 (GraphPad Software, Inc. CA). PCoA, ADONIS and PERMDISP tests (permutations = 999) of OTU distance/dissimilarity matrices were performed in QIIME, and PCoA plots were illustrated in R using the *ggplot2* package[91]. PCA was performed in R using the *ggbiplot* package[92]. Spearman's Rank correlations were performed in GraphPad Prism, whereas partial Spearman's Rank correlation analyses with adjustments for age and repeated measures correlation analyses were performed in R using the *ppcor*[29] and *rmcorr* packages[28], respectively. Heatmaps and hierarchically clustering of correlation coefficient were generated in R using the *gplots* package[93] and visualized in GraphPad Prism. Longitudinal metabolite and taxonomic abundance were modelled using LOESS regression, and implemented and plotted with 95% confidence intervals in R using the *ggplot2* package[91]. Longitudinal AhR activity was modelled used coarse LOWESS curve fits within the GraphPad Prism software. Two-tailed Student's *t* test (if normally distributed, evaluated by D'Agostino-Pearson test) or two-tailed non-parametric Mann-Whitney *U* test (if not normally distributed) were performed when comparing two groups. For comparison of more than two groups, statistical significance was evaluated by one-way ANOVA (if normally distributed) or the non-parametric Kruskal-Wallis test (if not normally distributed). P-values < 0.05 were considered statistically significant. When applicable p-values were corrected for multiple testing by the Benjamini–Hochberg false discovery rate (FDR)[94] using a cutoff of 0.1.

ACKNOWLEDGMENTS

We thank the children and families participating in the SKOT I study, which was supported by the Danish Directorate for Food, Fisheries and Agribusiness (Grant no. 3304-FSE-06-0503), as well as the children and parents participating in the CIG cohort. Furthermore, we thank Aarstiderne A/S for providing a small gift for the CIG participants. We thank Marlene Danner Dalgaard at the Technical University of Denmark in-house facility (DTU Multi-Assay Core, DMAC) for performing the 16S rRNA gene sequencing, MS-Omics (Hørsholm, Denmark) for performing the lactate analyses, Glycom A/S (Hørsholm, Denmark) for kindly donating the human milk oligosaccharides, and Anette Schnipper for her efforts in supporting the work. We also thank Satoru Fukiya and Atsushi

Yokota for providing *Bifidobacterium* gene manipulation tools and for technical suggestions, Yuta Sugiyama for helpful discussions on HPLC analysis, and Shingo Maeda for technical support on enzyme purification. This work was supported by Augustinus Fonden (grant no. 17-2003 to H.M.R.), Hørslev Fonden (grant no. 203866 to H.M.R.), Beckett Fonden (grant no. 17-2-0551 to H.M.R.), Aase og Ejnar Danielsens Fond (grant no. 10-002019 to H.M.R.), the Innovation Fund Denmark (grant no. 11-116163/0603-00487B; Center for Gut, Grain and Greens to T.R.L.), JSPS-KAKENHI (18K14379 to M.S., 19K22277 to T.K.), JSPS Overseas Research Fellowships (201860637 to M.S.) and the Institute for Fermentation, Osaka (to M.S. and T.K.) and "Diet-induced Arrangement of the gut Microbiome for improvement of Cardiometabolic health" (DINAMIC) under the Joint Programming Initiative, "A Healthy Diet for a Healthy Life" (JPI-HDHL), supported by the Innovation Fund Denmark (grant no. 5195-00001B to L.O.D.).

AUTHOR CONTRIBUTIONS

H.M.R. and M.F.L. conceived and designed the experiments. M.F.L. prepared the samples for sequencing/qPCR and analyzed the sequencing/qPCR data. H.M.R. prepared the samples for faecal and *in vitro* metabolome analyses and performed together with H.L.F. the targeted and untargeted metabolomics experiments. C.T.P. and L.O.D. performed the urine metabolomics. M.F.L. and M.S. performed the *in vitro* growth and mutant construction experiments. M.S. and T.K. performed enzyme kinetics. K.F.M. and C.M. designed the SKOT I study and M.V.L. managed the data. H.M.R. and M.F.L. designed the CIG cohort, recruited the study participants and managed the data. A.M.V. performed the AhR assays. N.B., D.A., U.M., A.R., and J.M.M. contributed to the interpretation of the results. S.B., W.A., T.K., M.I.B. and T.R.L. contributed with expert supervision. H.M.R. and M.F.L. led the work, undertook the integrative data analyses and drafted the manuscript. All authors contributed to and approved the final manuscript.

Data statement

Partial (V3 region) 16S rRNA gene amplicon sequencing data is deposited in the Sequence Read Archive (SRA) under the BioProjects PRJNA273694 (SKOT) and PRJNA554596 (CIG).

Competing Financial Interests statement

The authors declare no competing financial interests.

Corresponding authors

Henrik M. Roager
Tine R. Licht

REFERENCES

1. Victora, C. G. *et al.* Breastfeeding in the 21st century: epidemiology, mechanisms, and lifelong effect. *Lancet (London, England)* **387**, 475–90 (2016).
2. Horta, B. L., Loret de Mola, C. & Victora, C. G. Long-term consequences of breastfeeding on cholesterol, obesity, systolic blood pressure and type 2 diabetes: a systematic review and meta-analysis. *Acta Paediatr.* **104**, 30–7 (2015).
3. Laursen, M. F. *et al.* Infant Gut Microbiota Development Is Driven by Transition to Family Foods Independent of Maternal Obesity. *mSphere* **1**, e00069-15 (2016).
4. Bäckhed, F. *et al.* Dynamics and stabilization of the human gut microbiome during the first year of life. *Cell Host Microbe* **17**, 690–703 (2015).
5. Stewart, C. J. *et al.* Temporal development of the gut microbiome in early childhood from the TEDDY study. *Nature* **562**, 583–588 (2018).
6. Bode, L. The functional biology of human milk oligosaccharides. *Early Hum. Dev.* **91**, 619–622 (2015).
7. Gensollen, T., Iyer, S. S., Kasper, D. L. & Blumberg, R. S. How colonization by microbiota in early life shapes the immune system. *Science (80-.).* **352**, 539–544 (2016).
8. Stokholm, J. *et al.* Maturation of the gut microbiome and risk of asthma in childhood. *Nat. Commun.* **9**, 141 (2018).
9. Fujimura, K. E. *et al.* Neonatal gut microbiota associates with childhood multisensitized atopy and T cell differentiation. *Nat. Med.* **22**, 1187–1191 (2016).
10. Khosravi, A. & Mazmanian, S. K. Disruption of the gut microbiome as a risk factor for microbial infections. *Curr. Opin. Microbiol.* **16**, 221–227 (2013).
11. Fukuda, S. *et al.* Bifidobacteria can protect from enteropathogenic infection through production of acetate. *Nature* **469**, 543–547 (2011).
12. Roager, H. M. & Licht, T. R. Microbial tryptophan catabolites in health and disease. *Nat. Commun.* **9**, 3294 (2018).
13. Natividad, J. M. *et al.* Impaired Aryl Hydrocarbon Receptor Ligand Production by the Gut Microbiota Is a Key Factor in Metabolic Syndrome. *Cell Metab.* (2018). doi:10.1016/j.cmet.2018.07.001
14. Dodd, D. *et al.* A gut bacterial pathway metabolizes aromatic amino acids into nine circulating metabolites. *Nature* **551**, 648–652 (2017).
15. Guo, X. *et al.* Innate Lymphoid Cells Control Early Colonization Resistance against Intestinal Pathogens through ID2-Dependent Regulation of the Microbiota. *Immunity* **42**, 731–743 (2015).
16. Zelante, T. *et al.* Tryptophan catabolites from microbiota engage aryl hydrocarbon receptor

and balance mucosal reactivity via interleukin-22. *Immunity* **39**, 372–385 (2013).

17. Hoyles, L. *et al.* Molecular phenomics and metagenomics of hepatic steatosis in non-diabetic obese women. *Nat. Med.* **24**, 1070–1080 (2018).

18. Krishnan, S. *et al.* Gut Microbiota-Derived Tryptophan Metabolites Modulate Inflammatory Response in Hepatocytes and Macrophages. *Cell Rep.* **23**, 1099–1111 (2018).

19. Madsen, A. L., Schack-Nielsen, L., Larnkjaer, A., Mølgaard, C. & Michaelsen, K. F. Determinants of blood glucose and insulin in healthy 9-month-old term Danish infants; the SKOT cohort. *Diabet. Med.* **27**, 1350–7 (2010).

20. Kato, K. *et al.* Age-Related Changes in the Composition of Gut Bifidobacterium Species. *Curr. Microbiol.* **74**, 987–995 (2017).

21. Koga, Y. *et al.* Age-associated effect of kestose on Faecalibacterium prausnitzii and symptoms in the atopic dermatitis infants. *Pediatr. Res.* **80**, 844–851 (2016).

22. Li, X., Jiang, B., Pan, B., Mu, W. & Zhang, T. Purification and partial characterization of Lactobacillus species SK007 lactate dehydrogenase (LDH) catalyzing phenylpyruvic acid (PPA) conversion into phenyllactic acid (PLA). *J. Agric. Food Chem.* **56**, 2392–2399 (2008).

23. Koide, S., Iwata, S., Matsuzawa, H. & Ohta, T. Crystallization of allosteric L-lactate dehydrogenase from Thermus caldophilus and preliminary crystallographic data. *J. Biochem.* **109**, 6–7 (1991).

24. Takashi, M., So, I., Hiroshi, S., Haruhiko, M. & Takahisa, O. Sequence and characteristics of the Bifidobacterium longum gene encoding l-lactate dehydrogenase and the primary structure of the enzyme: a new feature of the allosteric site. *Gene* **85**, 161–168 (1989).

25. Bottacini, F. *et al.* Global transcriptional landscape and promoter mapping of the gut commensal Bifidobacterium breve UCC2003. *BMC Genomics* **18**, 991 (2017).

26. Hirayama, Y. *et al.* Development of a double-crossover markerless gene deletion system in Bifidobacterium longum: Functional analysis of the ??-galactosidase gene for raffinose assimilation. *Appl. Environ. Microbiol.* **78**, 4984–4994 (2012).

27. Matsumura, H., Takeuchi, A. & Kano, Y. Construction of Escherichia coli-Bifidobacterium longum shuttle vector transforming B. longum 105-A and 108-A. *Biosci. Biotechnol. Biochem.* **61**, 1211–2 (1997).

28. Bakdash, J. Z. & Marusich, L. R. Repeated Measures Correlation. *Front. Psychol.* **8**, 456 (2017).

29. Kim, S. ppcor: An R Package for a Fast Calculation to Semi-partial Correlation Coefficients. *Commun. Stat. Appl. methods* **22**, 665–674 (2015).

30. Alfa, M. J. *et al.* An Outbreak of Necrotizing Enterocolitis Associated with a Novel Clostridium Species in a Neonatal Intensive Care Unit. *Clin. Infect. Dis.* **35**, S101–S105 (2002).

31. Butel, M.-J. *et al.* Conditions of Bifidobacterial Colonization in Preterm Infants: A Prospective Analysis. *J. Pediatr. Gastroenterol. Nutr.* **44**, (2007).

32. Moles, L. *et al.* Bacterial Diversity in Meconium of Preterm Neonates and Evolution of Their Fecal Microbiota during the First Month of Life. *PLoS One* **8**, e66986 (2013).

33. Arboleya, S. *et al.* Establishment and development of intestinal microbiota in preterm neonates. *FEMS Microbiol. Ecol.* **79**, 763–772 (2012).

34. Korpela, K. *et al.* Intestinal microbiota development and gestational age in preterm neonates. *Sci. Rep.* **8**, 2453 (2018).

35. Cervantes-Barragan, L. *et al.* Lactobacillus reuteri induces gut intraepithelial CD4(+)CD8αα(+) T cells. *Science* eaah5825 (2017). doi:10.1126/science.aah5825

36. Tamburini, S., Shen, N., Wu, H. C. & Clemente, J. C. The microbiome in early life: implications for health outcomes. *Nat. Med.* **22**, 713–722 (2016).

37. Dominguez-Bello, M. G., Godoy-Vitorino, F., Knight, R. & Blaser, M. J. Role of the microbiome in human development. *Gut* **68**, 1108–1114 (2019).

38. Sakurai, T., Odamaki, T. & Xiao, J.-Z. Production of Indole-3-Lactic Acid by Bifidobacterium Strains Isolated fromHuman Infants. *Microorganisms* **7**, 340 (2019).

39. Yamada, C. *et al.* Molecular Insight into Evolution of Symbiosis between Breast-Fed Infants and a Member of the Human Gut Microbiome Bifidobacterium longum. *Cell Chem. Biol.* **24**, 515-524.e5 (2017).

40. Katayama, T. Host-derived glycans serve as selected nutrients for the gut microbe: human milk oligosaccharides and bifidobacteria. *Biosci. Biotechnol. Biochem.* **80**, 621–632 (2016).

41. Thomson, P., Medina, D. A. & Garrido, D. Human milk oligosaccharides and infant gut bifidobacteria: Molecular strategies for their utilization. *Food Microbiol.* **75**, 37–46 (2018).

42. Sakanaka, M. *et al.* Evolutionary adaptation in fucosyllactose uptake systems supports bifidobacteria-infant symbiosis. *Sci. Adv.* **5**, eaaw7696 (2019).

43. Vatanen, T. *et al.* The human gut microbiome in early-onset type 1 diabetes from the TEDDY study. *Nature* **562**, 589–594 (2018).

44. Natividad, J. M. *et al.* Impaired Aryl Hydrocarbon Receptor Ligand Production by the Gut Microbiota Is a Key Factor in Metabolic Syndrome. *Cell Metab.* **28**, 737-749.e4 (2018).

45. Metidji, A. *et al.* The Environmental Sensor AHR Protects from Inflammatory Damage by Maintaining Intestinal Stem Cell Homeostasis and Barrier Integrity. *Immunity* **49**, 353-362.e5 (2018).

46. Gomez de Aguero, M. *et al.* The maternal microbiota drives early postnatal innate immune development. *Science (80-.).* **351**, 1296–1302 (2016).

47. Kiss, E. A. *et al.* Natural Aryl Hydrocarbon Receptor Ligands Control Organogenesis of

Intestinal Lymphoid Follicles. *Science (80-.).* **334**, 1561–1565 (2011).

48. Qiu, J. *et al.* The Aryl Hydrocarbon Receptor Regulates Gut Immunity through Modulation of Innate Lymphoid Cells. *Immunity* **36**, 92–104 (2012).

49. Lamas, B. *et al.* CARD9 impacts colitis by altering gut microbiota metabolism of tryptophan into aryl hydrocarbon receptor ligands. *Nat. Med.* (2016). doi:10.1038/nm.4102

50. Hubbard, T. D. *et al.* Adaptation of the human aryl hydrocarbon receptor to sense microbiota-derived indoles. *Sci. Rep.* **5**, 12689 (2015).

51. Artis, D. & Spits, H. The biology of innate lymphoid cells. *Nature* **517**, 293–301 (2015).

52. Dant, T. A. *et al.* T-cell expression of AhR inhibits the maintenance of pT_{reg} cells in the gastrointestinal tract in acute GVHD. *Blood* **130**, 348–359 (2017).

53. Wilck, N. *et al.* Salt-responsive gut commensal modulates TH17 axis and disease. *Nature* **551**, 585–589 (2017).

54. Quintana, F. J. *et al.* Control of T(reg) and T(H)17 cell differentiation by the aryl hydrocarbon receptor. *Nature* **453**, 65–71 (2008).

55. Ning, Y. *et al.* Antibacterial activity of phenyllactic acid against Listeria monocytogenes and Escherichia coli by dual mechanisms. *Food Chem.* **228**, 533–540 (2017).

56. Rodríguez, N., Salgado, J. M., Cortés, S. & Domínguez, J. M. Antimicrobial activity of d-3-phenyllactic acid produced by fed-batch process against Salmonella enterica. *Food Control* **25**, 274–284 (2012).

57. Narayanan, T. K. & Rao, G. R. Beta-indoleethanol and beta-indolelactic acid production by Candida species: their antibacterial and autoantibiotic action. *Antimicrob. Agents Chemother.* **9**, 375–80 (1976).

58. Honoré, A. H. *et al.* Metabolic footprinting for investigation of antifungal properties of Lactobacillus paracasei. *Anal. Bioanal. Chem.* **408**, 83–96 (2016).

59. Peters, A. *et al.* Metabolites of lactic acid bacteria present in fermented foods are highly potent agonists of human hydroxycarboxylic acid receptor 3. *PLOS Genet.* **15**, e1008145 (2019).

60. Offermanns, S. Hydroxy-Carboxylic Acid Receptor Actions in Metabolism. *Trends Endocrinol. Metab.* **28**, 227–236 (2017).

61. Ahmed, K. *et al.* Deorphanization of GPR109B as a Receptor for the β-Oxidation Intermediate 3-OH-octanoic Acid and Its Role in the Regulation of Lipolysis. *J. Biol. Chem.* **284**, 21928–21933 (2009).

62. Irukayama-Tomobe, Y. *et al.* Aromatic D-amino acids act as chemoattractant factors for human leukocytes through a G protein-coupled receptor, GPR109B. *Proc. Natl. Acad. Sci.* **106**, 3930–3934 (2009).

63. Madsen, A. L., Larnkjær, A., Mølgaard, C. & Michaelsen, K. F. IGF-I and IGFBP-3 in healthy 9 month old infants from the SKOT cohort: Breastfeeding, diet, and later obesity. *Growth Horm. IGF Res.* **21**, 199–204 (2011).

64. Laursen, M. F. *et al.* Having older siblings is associated with gut microbiota development during early childhood. *BMC Microbiol.* **15**, 154 (2015).

65. Laursen, M. F., Dalgaard, M. D. & Bahl, M. I. Genomic GC-Content Affects the Accuracy of 16S rRNA Gene Sequencing Based Microbial Profiling due to PCR Bias. *Front. Microbiol.* **8**, 1934 (2017).

66. Laursen, M. F. *et al.* Administration of two probiotic strains during early childhood does not affect the endogenous gut microbiota composition despite probiotic proliferation. *BMC Microbiol.* **17**, 175 (2017).

67. Edgar, R. C. UPARSE: highly accurate OTU sequences from microbial amplicon reads. *Nat. Methods* **10**, 996–8 (2013).

68. Caporaso, J. G. *et al.* QIIME allows analysis of high-throughput community sequencing data. *Nat. Methods* **7**, 335–6 (2010).

69. Wang, Q., Garrity, G. M., Tiedje, J. M. & Cole, J. R. Naive Bayesian classifier for rapid assignment of rRNA sequences into the new bacterial taxonomy. *Appl. Environ. Microbiol.* **73**, 5261–7 (2007).

70. DeSantis, T. Z. *et al.* Greengenes, a chimera-checked 16S rRNA gene database and workbench compatible with ARB. *Appl. Environ. Microbiol.* **72**, 5069–72 (2006).

71. Altschul, S. F., Gish, W., Miller, W., Myers, E. W. & Lipman, D. J. Basic local alignment search tool. *J. Mol. Biol.* **215**, 403–410 (1990).

72. Frese, S. A. *et al.* Persistence of Supplemented Bifidobacterium longum subsp. infantis EVC001 in Breastfed Infants. (2017). doi:10.1128/mSphere

73. Lawley, B. *et al.* Differentiation of *Bifidobacterium longum* subspecies *longum* and *infantis* by quantitative PCR using functional gene targets. *PeerJ* **5**, e3375 (2017).

74. Sprenger, N., Lee, L. Y., De Castro, C. A., Steenhout, P. & Thakkar, S. K. Longitudinal change of selected human milk oligosaccharides and association to infants' growth, an observatory, single center, longitudinal cohort study. *PLoS One* **12**, e0171814 (2017).

75. Xu, G. *et al.* Absolute Quantitation of Human Milk Oligosaccharides Reveals Phenotypic Variations during Lactation. *J. Nutr.* **147**, 117–124 (2017).

76. Sakurama, H. *et al.* Lacto-N-biosidase encoded by a novel gene of bifidobacterium longum subspecies longum shows unique substrate specificity and requires a designated chaperone for its active expression. *J. Biol. Chem.* **288**, 25194–25206 (2013).

77. Sakanaka, M. *et al.* Functional analysis of bifidobacterial promoters in Bifidobacterium longum and Escherichia coli using the α-galactosidase gene as a reporter. *J. Biosci. Bioeng.*

118, 489–495 (2014).

78. Poolman, B., Nijssen, R. M. J. & Konings, W. N. Dependence of Streptococcus lactis phosphate transport on internal phosphate concentration and internal pH. *J. Bacteriol.* **169**, 5373–5378 (1987).

79. Barri, T., Holmer-Jensen, J., Hermansen, K. & Dragsted, L. O. Metabolic fingerprinting of high-fat plasma samples processed by centrifugation- and filtration-based protein precipitation delineates significant differences in metabolite information coverage. *Anal. Chim. Acta* **718**, 47–57 (2012).

80. Nielsen, L. N. *et al.* Glyphosate has limited short-term effects on commensal bacterial community composition in the gut environment due to sufficient aromatic amino acid levels. *Environ. Pollut.* **233**, (2018).

81. Roager, H. M. *et al.* Colonic transit time is related to bacterial metabolism and mucosal turnover in the gut. *Nat. Microbiol.* **1**, 16093 (2016).

82. Smith, C. A., Want, E. J., O'Maille, G., Abagyan, R. & Siuzdak, G. XCMS: Processing Mass Spectrometry Data for Metabolite Profiling Using Nonlinear Peak Alignment, Matching, and Identification. *Anal. Chem.* **78**, 779–787 (2006).

83. Sumner, L. W. *et al.* Proposed minimum reporting standards for chemical analysis Chemical Analysis Working Group (CAWG) Metabolomics Standards Initiative (MSI). *Metabolomics* **3**, 211–221 (2007).

84. Gürdeniz, G., Kristensen, M., Skov, T. & Dragsted, L. O. The Effect of LC-MS Data Preprocessing Methods on the Selection of Plasma Biomarkers in Fed vs. Fasted Rats. *Metabolites* **2**, 77–99 (2012).

85. Pluskal, T., Castillo, S., Villar-Briones, A. & Oresic, M. MZmine 2: modular framework for processing, visualizing, and analyzing mass spectrometry-based molecular profile data. *BMC Bioinformatics* **11**, 395 (2010).

86. van der Kloet, F. M., Bobeldijk, I., Verheij, E. R. & Jellema, R. H. Analytical error reduction using single point calibration for accurate and precise metabolomic phenotyping. *J. Proteome Res.* **8**, 5132–41 (2009).

87. Smart, K. F., Aggio, R. B. M., Houtte, J. V. R. Van & Villas-Bôas, S. G. Analytical platform for metabolome analysis of microbial cells using methyl chloroformate derivatization followed by gas chromatography-mass spectrometry. *Nat. Protoc.* **5**, 1709–1729 (2010).

88. Johnsen, L. G., Skou, P. B., Khakimov, B. & Bro, R. Gas chromatography – mass spectrometry data processing made easy. *J. Chromatogr. A* **1503**, 57–64 (2017).

89. Rosenmai, A. K. *et al.* Are structural analogues to bisphenol a safe alternatives? *Toxicol. Sci.* **139**, 35–47 (2014).

90. R Core Team. R: A language and environment for statistical computing. (2013).

91. Wickhamm, H. *ggplot2 Elegant Graphics for Data Analysis*. (Springer, New York, 2009).

92. Vu, V. ggbiplot: a ggplot2 based biplot. 2011

93. Warnes, G. R. *et al.* gplots: Various R Programming Tools for Plotting Data. R package version 2.16.0. *CRAN* (2015).

94. Benjamini, Y. & Hochberg, Y. Controlling the False Discovery Rate - a Practical and Powerful Approach to Multiple Testing. *J. R. Stat. Soc. Ser. B-Methodological* **57**, 289–300 (1995).

95. Smith, E. A. & Macfarlane, G. T. Enumeration of human colonic bacteria producing phenolic and indolic compounds: effects of pH, carbohydrate availability and retention time on dissimilatory aromatic amino acid metabolism. *J. Appl. Bacteriol.* **81**, 288–302 (1996).

96. Smith, E. A. & Macfarlane, G. T. Formation of Phenolic and Indolic Compounds by Anaerobic Bacteria in the Human Large Intestine. *Microb. Ecol.* **33**, 180–188 (1997).

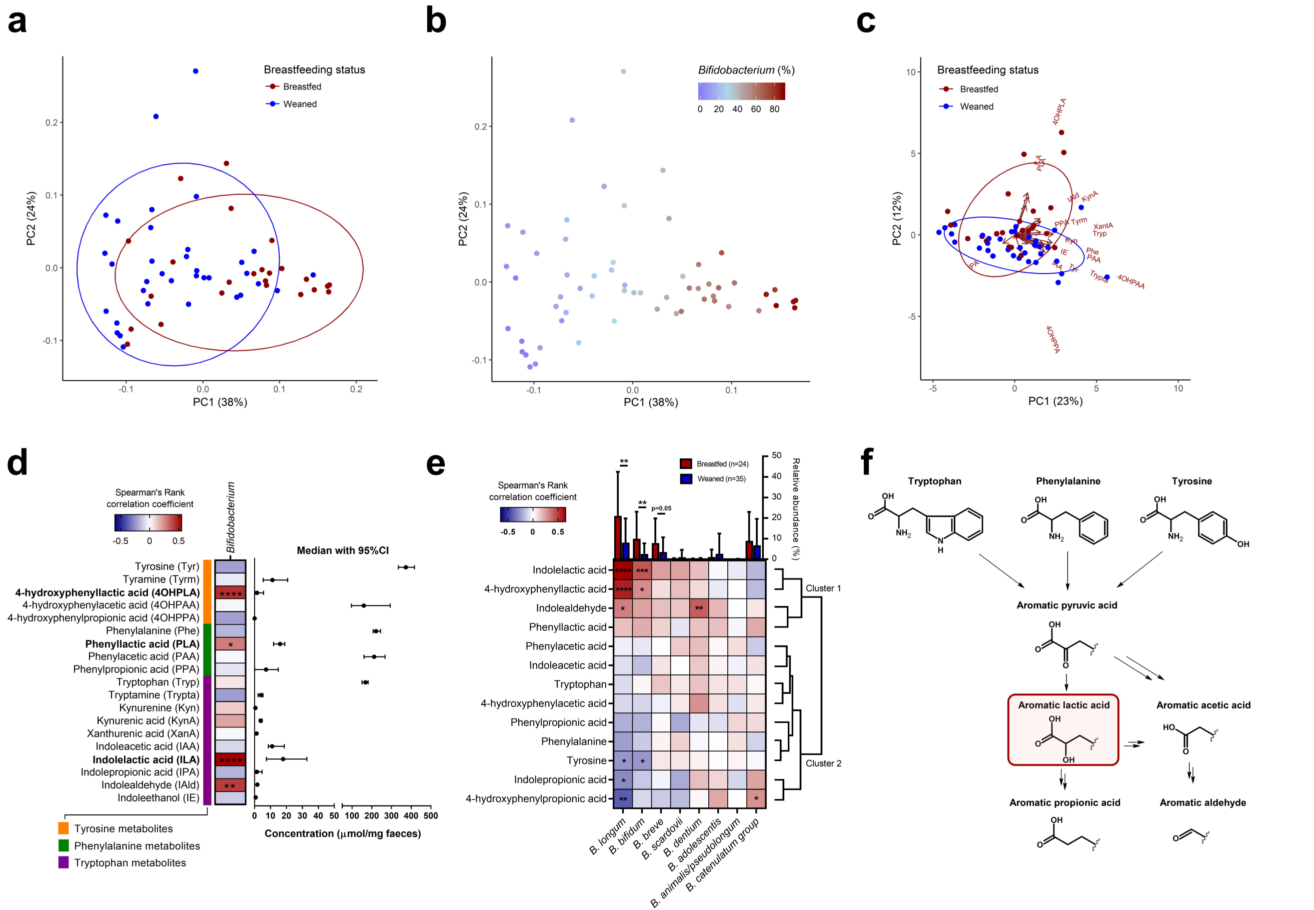

a
Breastfeeding status
Breastfed
Weaned
PC1 (38%)
PC2 (24%)
b
Bifidobacterium (%)
PC1 (38%)
PC2 (24%)
c
Breastfeeding status
Breastfed
Weaned
PC1 (23%)
PC2 (12%)
d
Spearman's Rank correlation coefficient
Bifidobacterium
Median with 95%CI
Tyrosine (Tyr)
Tyramine (Tyrm)
4-hydroxyphenyllactic acid (4OHPLA)
4-hydroxyphenylacetic acid (4OHPAA)
4-hydroxyphenylpropionic acid (4OHPPA)
Phenylalanine (Phe)
Phenyllactic acid (PLA)
Phenylacetic acid (PAA)
Phenylpropionic acid (PPA)
Tryptophan (Tryp)
Tryptamine (Trypta)
Kynurenine (Kyn)
Kynurenic acid (KynA)
Xanthurenic acid (XanA)
Indoleacetic acid (IAA)
Indolelactic acid (ILA)
Indolepropionic acid (IPA)
Indolealdehyde (IAld)
Indoleethanol (IE)
Concentration (μmol/mg faeces)
Tyrosine metabolites
Phenylalanine metabolites
Tryptophan metabolites
e
Spearman's Rank correlation coefficient
Breastfed (n=24)
Weaned (n=35)
Relative abundance (%)
p=0.05
Indolelactic acid
4-hydroxyphenyllactic acid
Indolealdehyde
Phenyllactic acid
Phenylacetic acid
Indoleacetic acid
Tryptophan
4-hydroxyphenylacetic acid
Phenylpropionic acid
Phenylalanine
Tyrosine
Indolepropionic acid
4-hydroxyphenylpropionic acid
Cluster 1
Cluster 2
B. longum
B. bifidum
B. breve
B. scardovii
B. dentium
B. adolescentis
B. animalis/pseudolongum
B. catenulatum group
f
Tryptophan
Phenylalanine
Tyrosine
Aromatic pyruvic acid
Aromatic lactic acid
Aromatic acetic acid
Aromatic propionic acid
Aromatic aldehyde

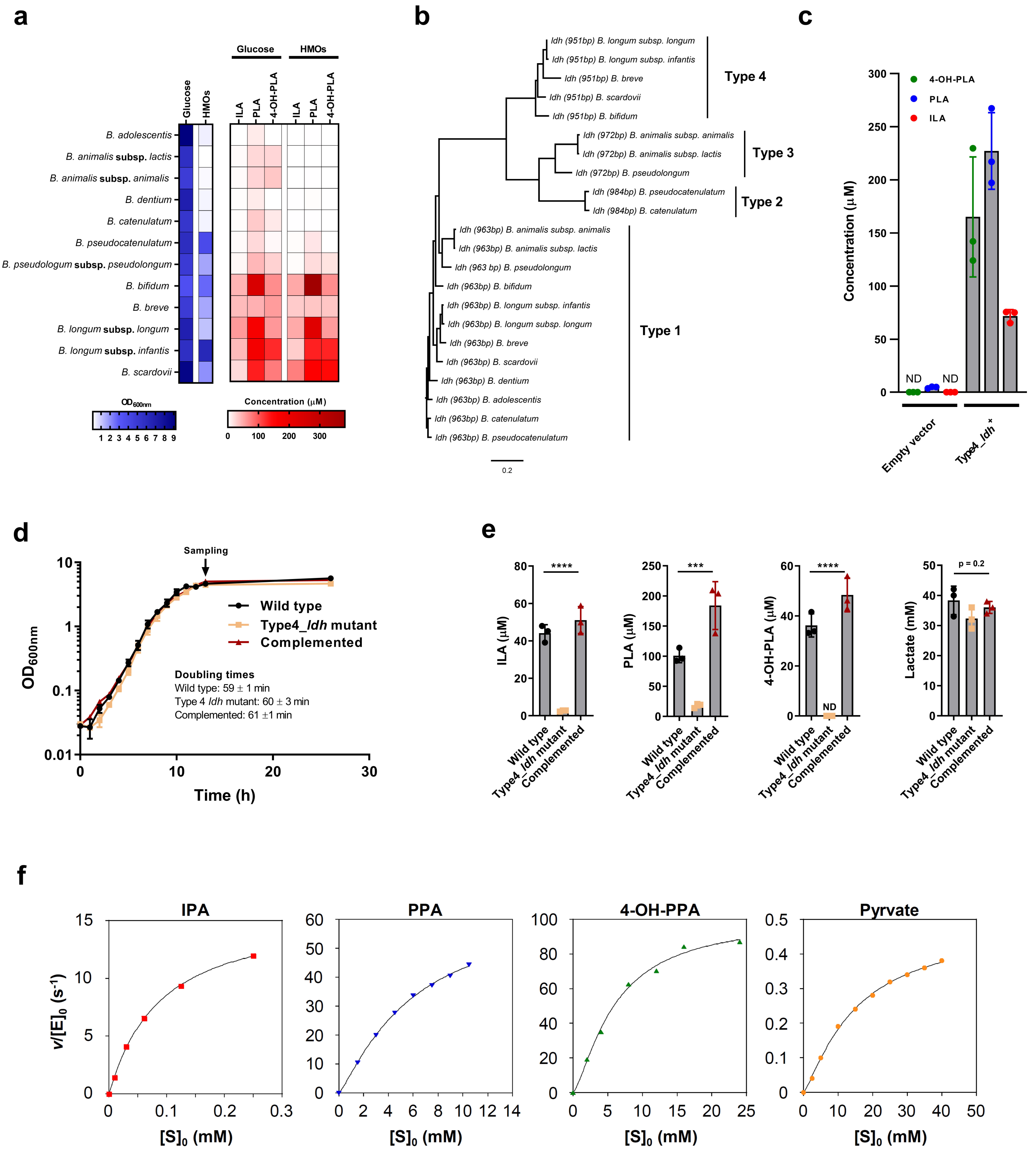

g

Kinetic parameters (Hill equation) of type 4 LDH

Substrate	$K_{0.5}$ (mM)	k_{cat} (s^{-1})	$k_{cat}/K_{0.5}$ (s^{-1} mM^{-1})	n_H (Hill coefficient)
IPA	0.08 ± 0.01	15.21 ± 1.01	193.73	1.05 ± 0.02
PPA	5.96 ± 0.06	64.22 ± 2.38	10.77	1.20 ± 0.01
4-OH-PPA	6.61 ± 0.93	103.89 ± 4.32	15.83	1.39 ± 0.01
Pyruvate	14.88 ± 0.48	0.47 ± 0.03	0.03	1.28 ± 0.05

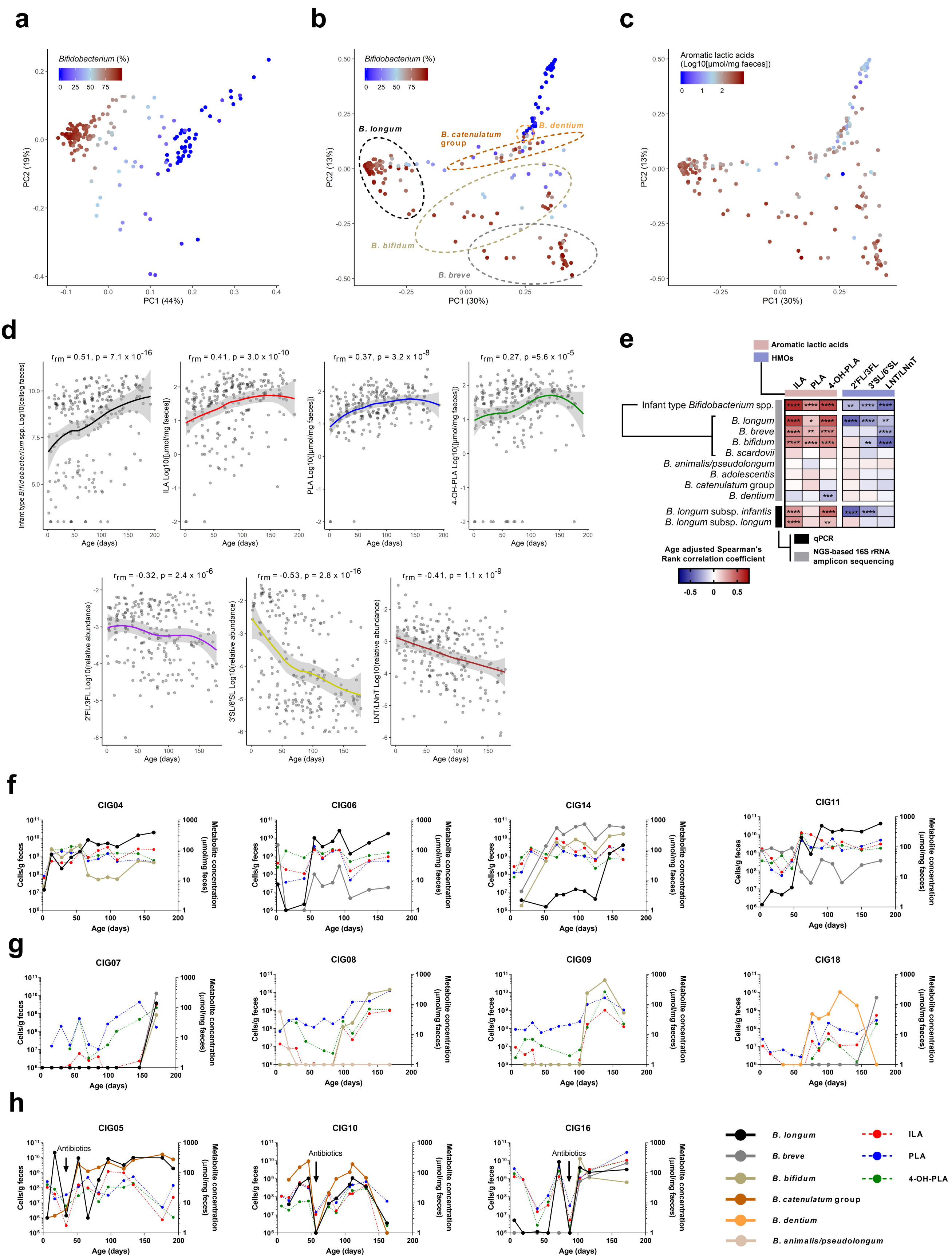

a
b
c
d
e
f
g
h
Bifidobacterium (%)
Aromatic lactic acids (Log10[µmol/mg faeces])
PC1 (44%)
PC2 (19%)
PC1 (30%)
PC2 (13%)
B. longum
B. catenulatum group
B. dentium
B. bifidum
B. breve
Aromatic lactic acids
HMOs
ILA
PLA
4-OH-PLA
2'FL/3FL
3'SL/6'SL
LNT/LNnT
Infant type Bifidobacterium spp.
B. scardovii
B. animalis/pseudolongum
B. adolescentis
B. longum subsp. infantis
B. longum subsp. longum
qPCR
NGS-based 16S rRNA amplicon sequencing
Age adjusted Spearman's Rank correlation coefficient
Age (days)
CIG04
CIG06
CIG14
CIG11
CIG07
CIG08
CIG09
CIG18
CIG05
CIG10
CIG16
Antibiotics
Cells/g feces
Metabolite concentration (µmol/mg feces)

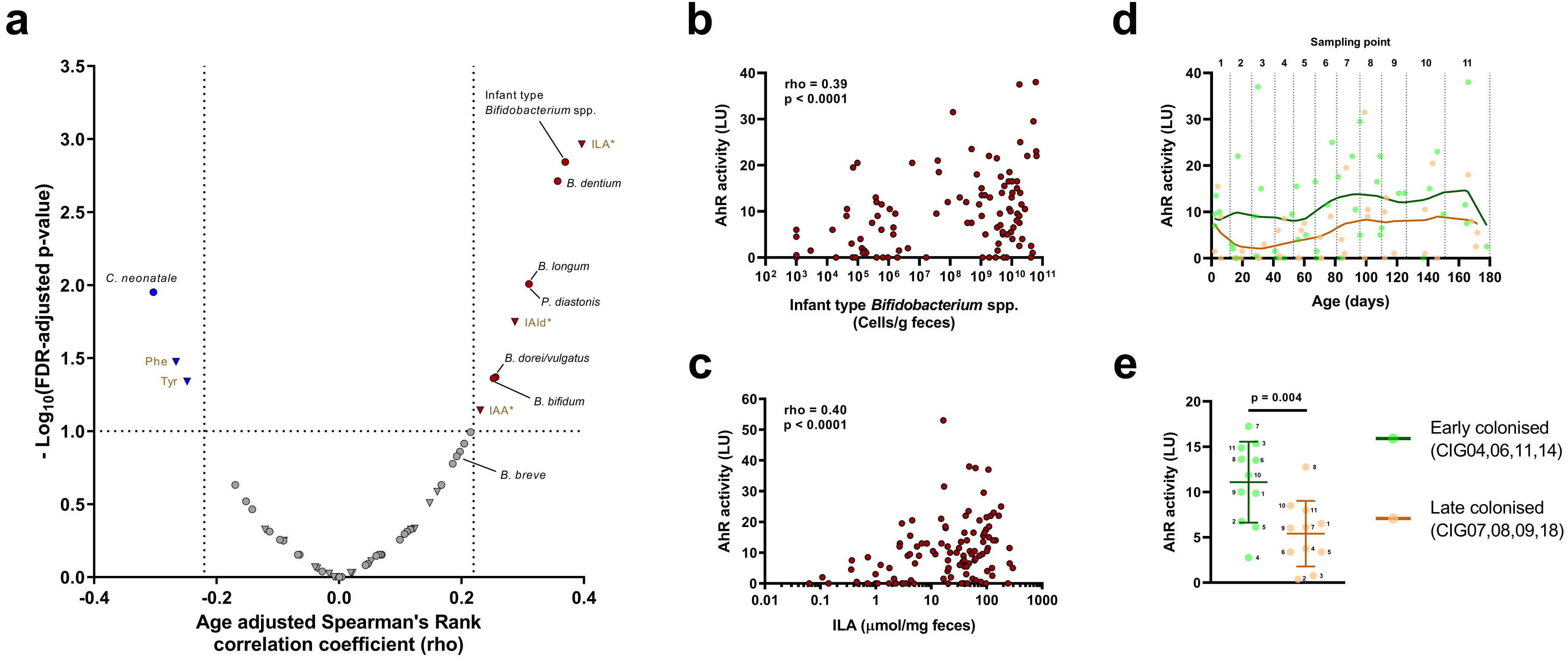

a
Infant type
Bifidobacterium spp.
ILA*
B. dentium
C. neonatale
B. longum
P. diastonis
IAld*
Phe
Tyr
B. dorei/vulgatus
B. bifidum
IAA*
B. breve
- Log10(FDR-adjusted p-value)
Age adjusted Spearman's Rank correlation coefficient (rho)
b
rho = 0.39
p < 0.0001
AhR activity (LU)
Infant type Bifidobacterium spp. (Cells/g feces)
c
rho = 0.40
p < 0.0001
AhR activity (LU)
ILA (µmol/mg feces)
d
Sampling point
AhR activity (LU)
Age (days)
e
p = 0.004
AhR activity (LU)
Early colonised (CIG04,06,11,14)
Late colonised (CIG07,08,09,18)